INTERNAL MEDICINE

□ CASE REPORT □

Bilateral Peripheral Infiltrates Refractory to Immunosuppressants were Diagnosed as Autoimmune Pulmonary Alveolar Proteinosis and Improved by Inhalation of Granulocyte/Macrophage-Colony Stimulating Factor

Hironori Satoh[1,2], Ryushi Tazawa[3], Tomohiro Sakakibara[1], Shinya Ohkouchi[1], Masahito Ebina[1], Makoto Miki[4], Koh Nakata[3] and Toshihiro Nukiwa[1,5]

Abstract

A 55-year-old non-smoking woman was admitted to our hospital for re-evaluation of unimproved peripheral ground-glass opacities despite prednisolone and cyclosporine treatment. She was diagnosed with autoimmune pulmonary alveolar proteinosis (PAP) based on transbronchial lung biopsy and granulocyte/macrophage colony-stimulating factor (GM-CSF) antibody testing. GM-CSF inhalation therapy markedly improved the opacities. Bilateral, centrally located lung opacities are typical in PAP, however 10 PAP cases with peripheral infiltration were reported in Japan recently, of which GM-CSF antibody was positive in six. To avoid inappropriate immunosuppressant treatment, PAP should be considered in the differential diagnosis of such peripheral opacities. GM-CSF antibody might be useful for diagnosis.

Key words: pulmonary alveolar proteinosis, subpleural infiltration, GM-CSF inhalation, GM-CSF antibody, steroid therapy

(Intern Med 51: 1737-1742, 2012)
(DOI: 10.2169/internalmedicine.51.6093)

Introduction

Pulmonary alveolar proteinosis (PAP), first described in 1958 (1) as a rare and severe lung disease characterized by the intra-alveolar accumulation of surfactant lipids and proteins, impairs gas exchange and results in progressive respiratory insufficiency. Currently, PAP is classifiable into four classes: congenital PAP, autoimmune (idiopathic) PAP, secondary PAP, and unclassified PAP. More than 90% of cases are diagnosed as autoimmune PAP (2). Patients with autoimmune PAP present high levels of autoantibodies against the granulocyte/macrophage colony-stimulating factor (GM-CSF) in the serum as well as in bronchoalveolar lavage fluid (2-6).

Findings from computed tomography (CT) studies of PAP include air space ground-glass interlobular and intralobular opacities and consolidation, which are distributed in a geographic or patchy pattern from the central to peripheral zones (7, 8). Usually, the distribution of PAP shadows is predominantly central: it is rarely peripheral. Furthermore, previous reports show that the peripheral shadows in PAP patients disappear without treatment (9, 10). Here, we describe a patient with autoimmune PAP showing peripheral ground-glass appearance that worsened during steroid and cyclosporine therapy, however it was improved with GM-CSF inhalation therapy.

[1]Department of Respiratory Medicine, Tohoku University Graduate School of Medicine, Japan, [2]Department of Medical Biochemistry, Tohoku University Graduate School of Medicine, Japan, [3]Bioscience Medical Research Center, Niigata University Medical and Dental Hospital, Japan, [4]Department of Respiratory Medicine, Japanese Red Cross Sendai Hospital, Japan and [5]South Miyagi Medical Center, Japan
Received for publication July 1, 2011; Accepted for publication March 19, 2012
Correspondence to Dr. Toshihiro Nukiwa, toshinkw47@gmail.com

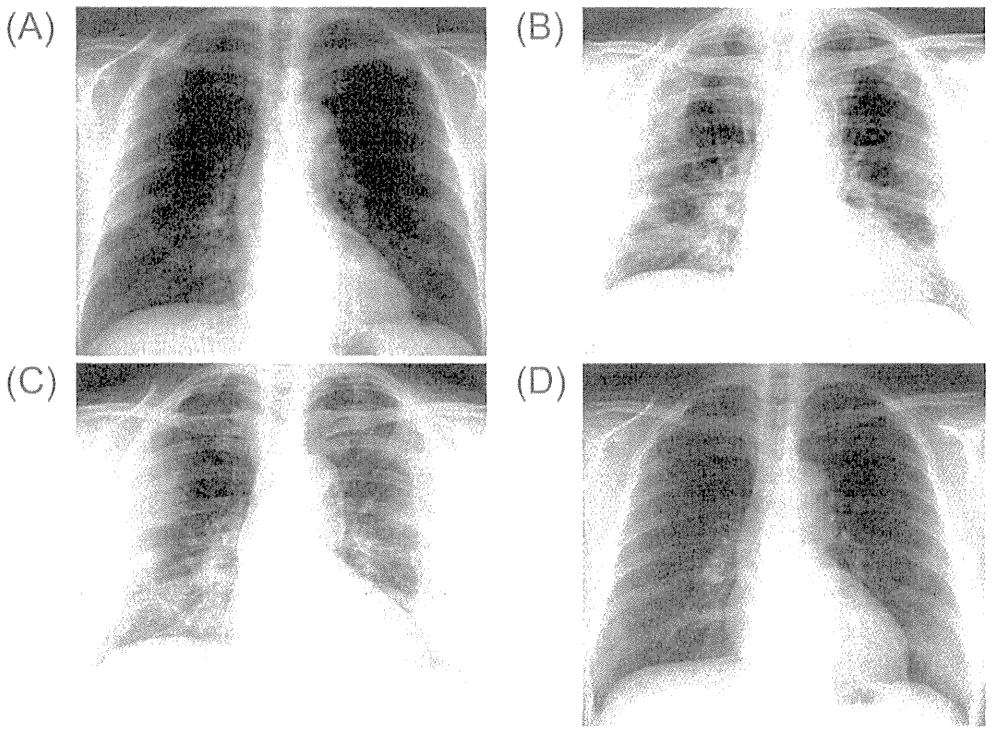

Figure 1. Chest radiograph from an annual check-up showing an abnormal shadow, predominantly in the bilateral peripheral lung field (A). The shadow worsened after prednisolone treatment (B) and worsened further after adding cyclosporine treatment (C). The shadow improved markedly after 6-month granulocyte/macrophage colony-stimulating factor (GM-CSF) inhalation therapy (D).

Case Report

A previously healthy 55-year-old non-smoking woman who had a normal chest radiograph at an annual health check-up 1 year previously was referred to our affiliated hospital because of the appearance of bilateral peripheral shadows on a chest radiograph in September 2004 (Fig. 1A). The patient was a homemaker without a remarkable family history. She had shortness of breath on exertion (Grade 1 of MRC Breathlessness Scale). A chest CT image revealed subpleural heterogeneous ground-glass opacities (GGOs) partially including consolidation and without definite interlobular thickening (Fig. 2A). Examination of the bronchoalveolar lavage fluid (BALF) revealed lymphocytosis (macrophages, 75.5% of total cells; lymphocytes, 23.5%; neutrophils, 1%) with no turbidity, no foamy macrophages, and no amorphous materials. Transbronchial lung biopsy (TBLB) yielded no specific or diagnostically helpful finding. A serum level of KL-6, a mucin-like glycoprotein, was 611 U/mL. Based on these findings, she was provisionally diagnosed with cryptogenic organizing pneumonia. Because the symptom did not improve during the initial observation, she was treated with oral prednisolone (0.5 mg/kg) for three months, but showed no clinical improvement. She was referred to our hospital in December 2004. The patient did not agree to undergo further examination and therefore was treated with prednisolone for 1 year. However, peripheral shadows on the chest radiograph worsened (Fig. 1B). Later, cyclosporine was added to her treatment for three months. The chest radiograph and CT findings worsened with time (Fig. 1C, 2B). She was admitted to our hospital for re-evaluation in December 2005.

Laboratory studies showed an elevated white blood cell count (11,600/μL), probably because of steroid therapy (Table 1). Serum levels of total bilirubin were elevated by an unknown cause. Levels of surfactant protein D (SP-D) (151.2 ng/mL) and KL-6 (1,176 U/mL) were increased significantly. Arterial blood gas analysis in room air revealed mild hypoxemia (partial pressure of oxygen (PaO_2), 67.6 Torr), indicating a significantly expanded alveolar-arterial oxygen gradient (A-aDO_2). Pulmonary function tests indicated normal respiratory functions. Electrocardiography indicated slight sinus tachycardia at 116 beats/min, perhaps associated with hypoxemia. A repeat of bronchoscopy revealed milky lavage fluid containing large foamy macrophages (macrophages, 84%; lymphocytes, 15%; neutrophils, 1%; Fig. 3A). The TBLB specimens showed that the alveoli with preserved lung architecture were filled with periodic acid-Schiff (PAS)-positive eosinophilic amorphous materials (Fig. 4). The serum was positive for GM-CSF antibody (41.3 μg/mL). Autoimmune PAP was diagnosed based on the detection of GM-CSF antibody in the serum.

Although prednisolone and cyclosporine were discontin-

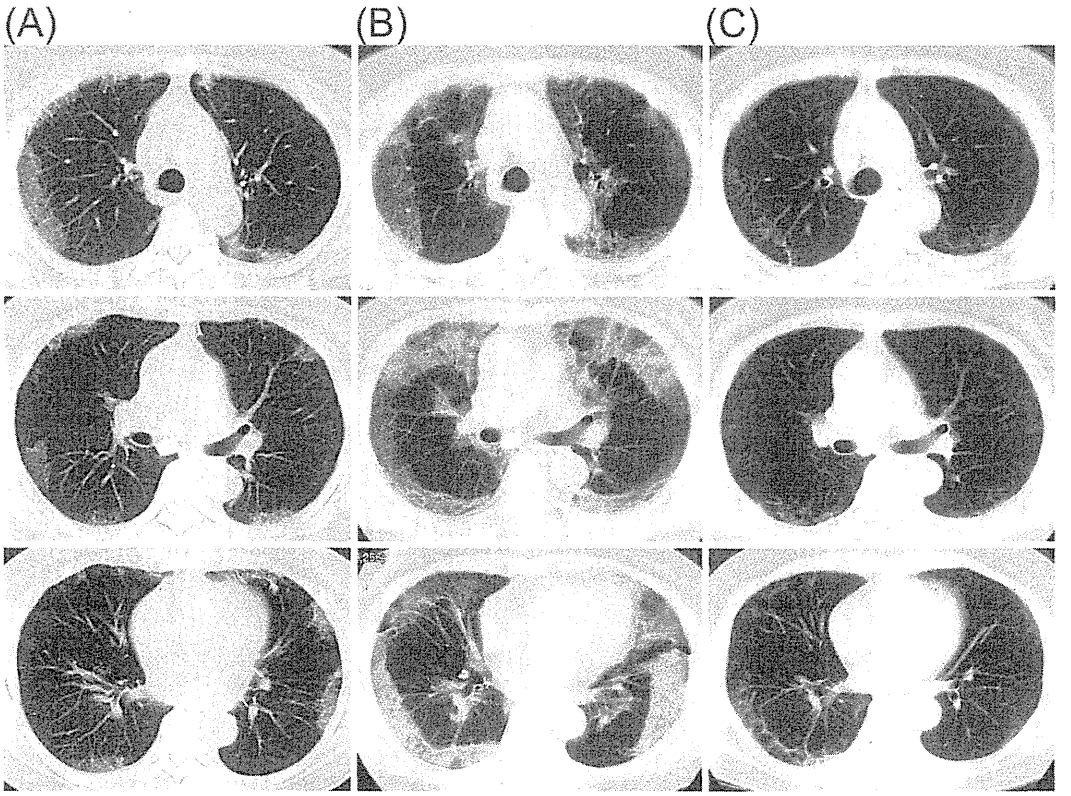

Figure 2. Chest computed tomography (CT) revealed peripheral ground-glass opacities (A), which worsened after oral prednisolone and cyclosporine regime (B) and improved markedly after 6-month GM-CSF inhalation therapy (C).

Table 1. Laboratory Data on Admission

<Hematology>						<Arterial blood gas>		
WBC	11,600	/μL	BUN	13	mg/dL	room air/at rest		
Seg	80	%	Cr	0.7	mg/dL	pH	7.45	
Lym	14	%	Na	146	mEq/L	$PaCO_2$	34.5	Torr
Eos	0	%	K	3.7	mEq/L	PaO_2	67.6	Torr
Bas	0	%	Cl	109	mEq/L	HCO_3	23.5	mmol/L
Mon	6	%	<Serology>			$AaDO_2$	39.0	Torr
RBC	4.88×10^6	/μL	CRP	0.1	mg/dL	<Pulmonary function test>		
Plt	257×10^3	/μL	KL-6	1,176	U/mL	%VC	88.4	%
<Blood chemistry>			SP-D	151.2	ng/mL	$FEV_{1.0\%}$	101	%
TP	6.2	g/dL	<BAL cell findings>			%DLco	104	%
T-Bil	3.2	mg/dL	Total cell	58.5×10^5	cells/mL			
AST	19	IU/L	AM	87	%			
ALT	16	IU/L	Lym	10	%			
LDH	252	IU/L	Neu	1	%			
ALP	121	IU/L	CD4/CD8	8.35				
γ-GTP	23	IU/L						

ued, the opacities did not improve during the subsequent 3-month observation. The patient was treated with GM-CSF inhalation of high-dose administration (sargramostim, 125 μg twice daily on Days 1-8, and none on Days 9-14) for six 2-week cycles and consequent low dose administration months (125 μg once daily on Days 1-4, none on Days 5-14) for six 2-week cycles, using a jet nebulizer (LC Plus; PARI GmbH, Starnberg, Germany) which generates particles of mean mass aerodynamic diameter of 3.97-5.25 μm at a flow rate of 3-6 L/min, according to the manufacturer's instructions (11). The peripheral shadows on the chest radiograph and CT as well as bronchoscopic findings showed marked improvement (Fig. 1D, 2C, 3B), and serum levels of SP-D and KL-6 decreased. Amorphous materials had markedly decreased in BALF (macrophages, 89%; lymphocytes, 10%; neutrophils, 1%). No recurrence was observed during

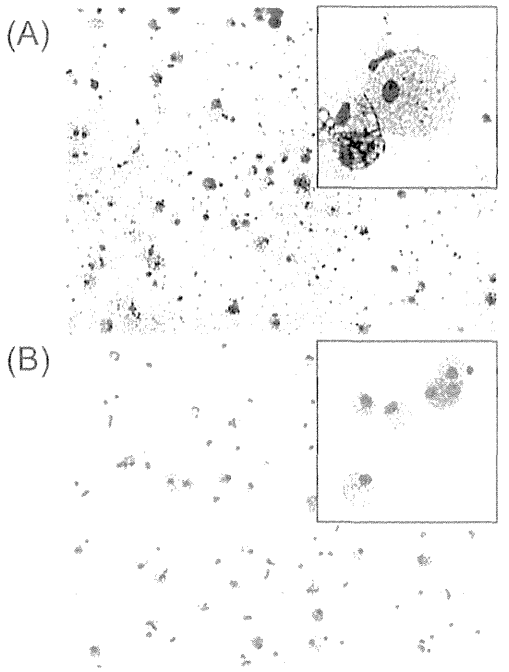

Figure 3. Wright-Giemsa staining of the cells in the bronchoalveolar lavage fluid before (A) and after (B) GM-CSF inhalation therapy (×200). Insets show the cells at a higher magnification (×400). The extracellular proteinaceous material and cell debris decreased markedly after 6-month GM-CSF inhalation therapy. The number of foamy macrophages decreased, although that of smaller alveolar macrophages increased after treatment.

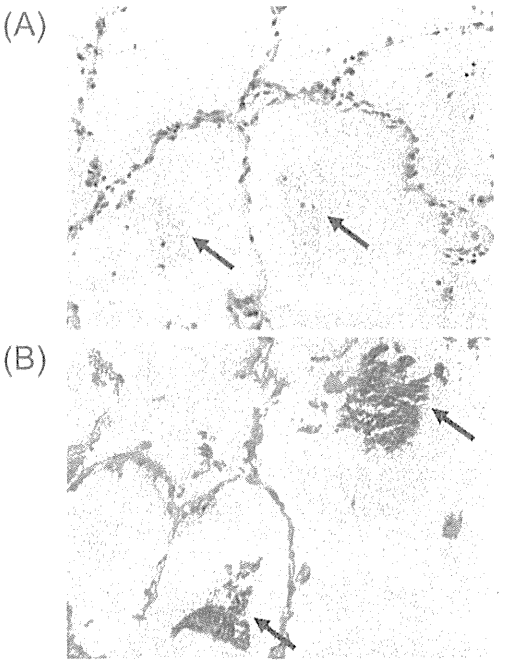

Figure 4. Hematoxylin and Eosin staining of lung tissue during transbronchial lung biopsy (TBLB; ×200) (A), showing accumulation of proteinaceous materials within alveolar spaces. Periodic acid-Schiff (PAS) staining of lung tissue during TBLB (×200) shows that the amorphous material is PAS-positive (B). Arrows indicate PAS-positive materials.

the five years following treatment. However, the serum level of GM-CSF antibody was still elevated (19.5 μg/mL) five years after the end of the GM-CSF inhalation therapy.

Discussion

A typical CT finding of PAP is a "crazy-paving appearance," distributed centrally in both lungs. Instead, the present case showed bilateral GGOs localized in peripheral subpleural areas from the basal to the apical segments. Ten Japanese cases of PAP with subpleural infiltrates on CT findings have been reported in the Japanese and English literature. Most patients had no symptoms, and their condition did not worsen without treatment (Table 2) (9, 10, 12-19). Eight out of ten patients had never been a smoker.

The 10 cases yielded CT images of two types. One type showed solitary pulmonary nodule (20), as in Cases 5 (a nodule of 30 mm in diameter), 8 (nodules, not referred), and 10 (a nodule of 40×20 mm). In these cases, lung cancer was suspected. Then they underwent surgical resection under video-assisted thoracoscopy. Cases 5, 8 and 10 were diagnosed pathologically as PAP. However, GM-CSF antibody was not measured in two of the cases. Case 8 demonstrated multiple nodular lesions, of which one lesion was diagnosed as bronchoalveolar carcinoma; the rest were pulmonary alveolar proteinosis. It is particularly interesting that Case 8 demonstrated positive GM-CSF antibody. The other was GGO distributed in the subpleural area, which the remaining seven cases showed. Six of the seven were female. GM-CSF antibody was measured in five of the seven cases: all five were positive. Case 4 worsened two years later, but the others remained stable.

In patients with PAP, infiltrates often disappear from the peripheral region to the central region (1). Mohri et al. (14) speculated that the GGOs might extend from the periphery to the central region and develop into air space consolidation as respiratory symptoms occur, suggesting that patients with peripheral GGOs might be exhibiting early stages of PAP. In this regard, the present case developed GGOs that extend from the peripheral to the central region and which disappeared from the central area toward the peripheral region. Recently, it has been demonstrated that GM-CSF administration by subcutaneous injection (21, 22) or inhalation (2, 4, 11) improved the respiratory function as well as CT findings of autoimmune PAP patients. Inhaled GM-CSF might first reach the mildly-impaired, proximal region in the lungs and improve the function of the macrophages present in those locations. The restored function of these alveolar macrophages may contribute to improving the clearance in the adjacent, distal regions. The present report describes exacerbation and improvement of peripheral infiltrates of a PAP patient in a series of CT, supporting the speculations

Table 2. Summary of Japanese Pulmonary Alveolar Proteinosis (PAP) Patients Showing Peripheral Ground-glass Opacities on CT Images

Case No.	Age (y)	Gender	Smoking history	Dust exposure	Symp -toms	BAL appearance Lymphocyte	GM-CSF antibody	Therapeutic history	Prognosis	Reference
1	39	F	Never	None	No	n.a. 11.5%	n.a.	None	7 mo stable	Inui *et al.* (9)
2	38	F	n.a.	n.a.	No	n.a.	n.a.	None	12 mo stable	Mita *et al.* (12)
3	55	F	Never	n.a.	No	Milk like 20%	Positive (BAL)	None	Recurrence after 2 y	Sugimoto *et al.* (13)
4	32	F	Never	None	No	Milk like 25.6%	Positive (BAL& Serum)	None	15 mo partially improved	Mohri *et al.* (14)
5	70	M	Current	Asbestos	No	n.a.	n.a.	(Resection for diagnosis)	3 y stable	Norikane *et al.* (15)
6	56	F	Never	n.a.	No	n.a.	Positive (Serum)	AM	No recurrence	Yamasaki *et al.* (16)
7	45	M	Never	None	No	n.a. 82%	Positive (Serum)	None	No recurrence for 3 y	Toyama *et al.* (17)
8	58	F	Never	None	No	n.a.	Positive (Serum)	(Resection for diagnosis)+AM	No recurrence for 3 y	Taniguchi *et al.* (18)
9	65	F	Never	None	No	n.a.	Positive	None	18 mo stable	Haga *et al.* (10)
10	57	M	Never	n.a.	No	n.a.	n.a.	(Resection for diagnosis)	No recurrence for 1 y	Sunadome *et al.* (19)

Key: n.a., not available; AM, ambroxol hydrochloride

described by Mohri et al. (14).

Although whole-lung lavage (WLL) has been the standard therapy for PAP, the recent perspective of the pathophysiology of PAP is leading us to innovative treatment options including GM-CSF administration, plasmapheresis and B-cell depletion. GM-CSF inhalation could be considered as an alternative in patients refractory to WLL, with a contraindication to general anesthesia during WLL, or under the effects of immunosuppressants, as in the present case. The treatment options will become more defined, as our knowledge in this field including CT patterns advances.

The present case worsened after steroid therapy. Cyclosporine, which was added on the expectation of improving organizing pneumonia refractory to 1-year steroid treatment (23), might also be associated with the worsening in chest radiographs during its administration. It is notable that Case 3 worsened as well after prednisolone therapy for autoimmune hemolytic anemia as well (17). Careful consideration should be devoted to steroid administration in the treatment of autoimmune PAP because of its lack of efficacy and its associated risk. Reportedly, steroid therapy increases the production of phospholipids (24) and down-regulates monocyte function (25). To prevent inappropriate application of immunosuppressants, it is important to consider PAP in the differential diagnosis of such peripheral opacities, which requires detailed characterization of HRCT findings and serum markers. In this regard, GM-CSF antibody might be helpful for diagnosis.

In conclusion, PAP should be considered in the differential diagnosis of peripheral subpleural opacities. Measurement of GM-CSF antibody might be a useful diagnostic option. GM-CSF inhalation therapy improved the peripheral opacities observed on CT images of PAP patients.

The authors state that they have no Conflict of Interest (COI).

Acknowledgement

The authors thank Dr. Bruce C. Trapnell for critical reading of the manuscript.

References

1. Rosen SH, Castleman B, Liebow AA. Pulmonary alveolar proteinosis. N Engl J Med **258**: 1123-1142, 1958.
2. Tazawa R, Hamano E, Arai T, et al. Granulocyte-macrophage colony-stimulating factor and lung immunity in pulmonary alveolar proteinosis. Am J Respir Crit Care Med **171**: 1142-1149, 2005.
3. Arai T, Hamano E, Inoue Y, et al. Serum neutralizing capacity of GM-CSF reflects disease severity in a patient with pulmonary alveolar proteinosis successfully treated with inhaled GM-CSF. Respir Med **98**: 1227-1230, 2004.
4. Wylam ME, Ten R, Prakash UB, Nadrous HF, Clawson ML, Anderson PM. Aerosol granulocyte-macrophage colony-stimulating factor for pulmonary alveolar proteinosis. Eur Respir J **27**: 585-593, 2006.
5. Yamamoto H, Yamaguchi E, Agata H, et al. A combination therapy of whole lung lavage and GM-CSF inhalation in pulmonary alveolar proteinosis. Pediatr Pulmonol **43**: 828-830, 2008.
6. Tanaka N, Watanabe J, Kitamura T, Yamada Y, Kanegasaki S, Nakata K. Lungs of patients with idiopathic pulmonary alveolar proteinosis express a factor which neutralizes granulocyte-macrophage colony stimulating factor. FEBS Lett **442**: 246-250, 1999.
7. Trapnell BC, Whitsett JA, Nakata K. Pulmonary alveolar proteino-

sis. N Engl J Med **349**: 2527-2539, 2003.
8. Seymour JF, Presneill JJ. Pulmonary alveolar proteinosis: progress in the first 44 years. Am J Respir Crit Care Med **166**: 215-235, 2002.
9. Inui N, Chida K, Suda T, et al. A case of pulmonary alveolar proteinosis presenting with peripheral infiltrates. Nihon Kokyuki Gakkai Zasshi **37**: 333-336, 1999 (in Japanese).
10. Haga T, Kasamatsu N, Kobayashi T, Shibata M, Ogasawara T, Hashizume I. A case of pulmonary alveolar proteinosis presenting with peripheral ground-glass opacitiy. Nihon Kokyuki Gakkai Zasshi **47**: 71-75, 2009 (in Japanese).
11. Tazawa R, Trapnell BC, Inoue Y, et al. Inhaled granulocyte/macrophage-colony stimulating factor as therapy of pulmonary alveolar proteinosis. Am J Respir Crit Care Med **181**: 1345-1354, 2010.
12. Mita Y, Dobashi K, Shimizu Y, Nakazawa T, Mori M. Pulmonary alveolar proteinosis manifested by patchy peripheral air-space disease: a case report. Kitakanto Med J **53**: 285-287, 2003 (in Japanese).
13. Sugimoto C, Kobayashi H, Kanoh S, Motoyoshi K, Aida S. Radiological findings in initial pulmonary alveolar proteinosis detected in the post-treatment course of nocardiosis. Nihon Kokyuki Gakkai Zasshi **44**: 738-741, 2006 (in Japanese).
14. Mohri K, Miyashita N, Obase Y, et al. Pulmonary alveolar preoteinosis with bilateral ground-glass opacities localized in subpleural areas. The Journal of the Japan Society for Respiratory Endoscopy **29**: 275-278, 2007 (in Japanese).
15. Norikane S, Kato K, Kojima K, et al. A case of pulmonary alveolar proteinosis that showed localized ground glass attenuation. Rinsho Houshasen **53**: 660-663, 2008.
16. Yamasaki K, Yoshii C, Nishida C, et al. Early case of idiopathic pulmonary alveolar proteinosis positive for serum anti-GM-CSF antibody. Nihon Kokyuki Gakkai Zasshi **46**: 712-716, 2008 (in Japanese).
17. Toyama S, Ikari J, Konishi K, Okabe H, Tomita K, Nakamura H. A case of idiopathic pulmonary alveolar proteinosis with atypical CT findings. Kokyu **27**: 406-407, 2008 (in Japanese).
18. Taniguchi H, Abo H, Touge M, et al. A case of idiopathic pulmonary alveolar proteinosis with multiple localized ground-glass opacities. Arerugi **57**: 1061-1066, 2008 (in Japanese).
19. Sunadome H, Nohara J, Noguchi T, et al. A case of pulmonary alveolar proteinosis that showed solitary ground-glass opacity in the subpleural area. Nihon Kokyuki Gakkai Zasshi **48**: 516-519, 2010 (in Japanese).
20. Hansell DM, Armstrong P, Lynch DA, McAdams HP. Solitary pulmonary nodule. In: Imaging of the Diseases of the Chest. 4th. Elsevier Mosby, Philadelphia, 2005: 107-120.
21. Seymour JF, Presneill JJ, Schoch OD, et al. Therapeutic efficacy of granulocyte-macrophage colony-stimulating factor in patients with idiopathic acquired alveolar proteinosis. Am J Respir Crit Care Med **163**: 524-531, 2001.
22. Kavuru MS, Sullivan EJ, Piccin R, Thomassen MJ, Stoller JK. Exogenous granulocyte-macrophage colony-stimulating factor administration for pulmonary alveolar proteinosis. Am J Respir Crit Care Med **161**: 1143-1148, 2000.
23. Koinuma D, Miki M, Ebina M, et al. Successful treatment of a case with rapidly progressive bronchiolitis obliterans organizing pneumonia (BOOP) using cyclosporin A and corticosteroid. Intern Med **41**: 26-29, 2002.
24. Wilson DO, Rogers RM. Prolonged spontaneous remission in a patient with untreated pulmonary alveolar proteinosis. Am J Med **82**: 1014-1016, 1987.
25. Rinehart JJ, Sagone AL, Balcerzak SP, Ackerman GA, LoBuglio AF. Effects of corticosteroid therapy on human monocyte function. N Engl J Med **292**: 236-241, 1975.

The Journal of Immunology

Runx1 Deficiency in CD4$^+$ T Cells Causes Fatal Autoimmune Inflammatory Lung Disease Due to Spontaneous Hyperactivation of Cells

Won Fen Wong, Kazuyoshi Kohu, Akira Nakamura, Masahito Ebina, Toshiaki Kikuchi, Ryushi Tazawa, Keisuke Tanaka, Shunsuke Kon, Tomo Funaki, Akiko Sugahara-Tobinai, Chung Yeng Looi, Shota Endo, Ryo Funayama, Mineo Kurokawa, Sonoko Habu, Naoto Ishii, Manabu Fukumoto, Koh Nakata, Toshiyuki Takai and Masanobu Satake

J Immunol 2012; 188:5408-5420; Prepublished online 2 May 2012;
doi: 10.4049/jimmunol.1102991
http://www.jimmunol.org/content/188/11/5408

The Journal of Immunology is published twice each month by
The American Association of Immunologists, Inc.,
9650 Rockville Pike, Bethesda, MD 20814-3994.

Print ISSN: 0022-1767 Online ISSN: 1550-6606.

Runx1 Deficiency in CD4$^+$ T Cells Causes Fatal Autoimmune Inflammatory Lung Disease Due to Spontaneous Hyperactivation of Cells

Won Fen Wong,* Kazuyoshi Kohu,* Akira Nakamura,[†,‡] Masahito Ebina,[§] Toshiaki Kikuchi,[§] Ryushi Tazawa,[¶] Keisuke Tanaka,* Shunsuke Kon,* Tomo Funaki,* Akiko Sugahara-Tobinai,[†] Chung Yeng Looi,[†] Shota Endo,[†] Ryo Funayama,[‖] Mineo Kurokawa,[#] Sonoko Habu,[**] Naoto Ishii,[††] Manabu Fukumoto,[‡‡] Koh Nakata,[¶] Toshiyuki Takai,[†] and Masanobu Satake*

The Runx1 transcription factor is abundantly expressed in naive T cells but rapidly downregulated in activated T cells, suggesting that it plays an important role in a naive stage. In the current study, *Runx1*$^{-/-}$*Bcl2*^{tg} mice harboring Runx1-deleted CD4$^+$ T cells developed a fatal autoimmune lung disease. CD4$^+$ T cells from these mice were spontaneously activated, preferentially homed to the lung, and expressed various cytokines, including IL-17 and IL-21. Among these, the deregulation of *IL-21* transcription was likely to be associated with Runx binding sites located in an *IL-21* intron. IL-17 produced in Runx1-deleted cells mobilized innate immune responses, such as those promoted by neutrophils and monocytes, whereas IL-21 triggered humoral responses, such as plasma cells. Thus, at an initial stage, peribronchovascular regions in the lung were infiltrated by CD4$^+$ lymphocytes, whereas at a terminal stage, interstitial regions were massively occupied by immune cells, and alveolar spaces were filled with granular exudates that resembled pulmonary alveolar proteinosis in humans. Mice suffered from respiratory failure, as well as systemic inflammatory responses. Our data indicate that Runx1 plays an essential role in repressing the transcription of cytokine genes in naive CD4$^+$ T cells and, thereby, maintains cell quiescence. *The Journal of Immunology*, **2012, 188: 5408–5420.**

Activation of peripheral T cells by Ag engagement triggers their rapid expansion and the gain of effector functions. However, after Ag elimination, these cells are exhausted and destined to apoptotic cell death. When in a quiescent stage without any Ag stimulation, naive T cells consume less energy and are capable of existing for long periods in peripheral tissues, thus maintaining the diversity of their Ag-recognizing repertoire (1).

To maintain the quiescence state of T cells, intricate controls by intrinsic transcription factors, such as Klf2, Tob, Slfn2, Foxo, Foxp1, and Tsc1 (2–8), or extrinsic factors, such as regulatory T cells (Treg) (9), are pivotal. Failure of the quiescence controls can be caused by the deletion of quiescence-associated transcription factors or by defects in Treg activity. Under these circumstances, T cells are spontaneously hyperactivated and release excessive amounts of cytokines, which can cause a cytokine storm and often develop into systemic inflammatory response syndrome (SIRS) (10). Such a breakdown of immune tolerance is deleterious to the host. However, a full picture of intrinsic quiescence-control mechanisms for T cells remains elusive.

The Runx1 transcription factor is one of the key factors that drives various aspects of T cell differentiation through interplay with distinct molecules (11). In Th cell differentiation, interaction of Runx1 with Gata3 suppresses *IL-4* secretion and induces *IFN-γ* production (12). In addition, Runx1 transactivates *IL-17* through cooperative binding with ROR-γt (13), but it also inhibits *IL-17* when forming a complex with T-bet or Foxp3 (13, 14). In the differentiation of Treg, the interaction of Runx1 with Foxp3 is important for the continuous expression of the *Foxp3* gene, which ensures maintenance of a Treg phenotype (15, 16). Treg-specific deletion of Runx1 or core-binding factor β (CBFβ; a cofactor of the Runx family) in two independent mice models caused colitis or pneumonitis, respectively (17, 18).

We previously observed that Runx1 is highly expressed in naive CD4$^+$ T cells but is rapidly turned off upon T cell activation (19). Runx1 downregulation during T cell activation appears crucial for

*Department of Molecular Immunology, Institute of Development, Aging and Cancer, Tohoku University, Sendai 980-8575, Japan; [†]Department of Experimental Immunology, Institute of Development, Aging and Cancer, Tohoku University, Sendai 980-8575, Japan; [‡]Department of Immunology, Kanazawa Medical School, Ishikawa 920-0293, Japan; [§]Department of Pulmonary Medicine, Tohoku University Graduate School of Medicine, Sendai 980-8574, Japan; [¶]Bioscience Medical Research Center, Niigata University Medical and Dental Hospital, Niigata 951-8520, Japan; [‖]Division of Cell Proliferation, Tohoku University Graduate School of Medicine, Sendai 980-8575, Japan; [#]Department of Hematology and Oncology, Graduate School of Medicine, University of Tokyo, Tokyo 113-8655, Japan; [**]Department of Immunology, Juntendo University School of Medicine, Tokyo 113-8421, Japan; [††]Department of Immunology, Tohoku University Graduate School of Medicine, Sendai 980-8575, Japan; and [‡‡]Department of Pathology, Institute of Development, Aging and Cancer, Tohoku University, Sendai 980-8575, Japan

Received for publication October 17, 2011. Accepted for publication March 28, 2012.

This work was supported by grants-in-aid for scientific research from the Japan Society for the Promotion of Science and a research grant from the Ministry of Education, Science, Sports, Culture and Technology, Japan. W.F.W. is a Japan Society for the Promotion of Science postdoctoral fellow. N.I., T.T., and M.S. are members of the Global Center of Excellence program "Network Medicine" at Tohoku University.

Address correspondence and reprint requests to Dr. Masanobu Satake, Institute of Development, Aging and Cancer, Tohoku University, Seiryo-machi 4-1, Aoba-ku, Sendai 980-8575, Japan. E-mail address: satake@idac.tohoku.ac.jp

The online version of this article contains supplemental material.

Abbreviations used in this article: BALF, bronchoalveolar lavage fluid; *Bcl2*^{tg}, Bcl2 transgenic; BM, bone marrow; CBFβ, core binding factor β; ChIP, chromatin immunoprecipitation; CNS, conserved noncoding sequence; EM, Elastica-Masson; GC, germinal center; HS, hypersensitive site; mLN, mediastinal lymph node; P, promoter; PAP, pulmonary alveolar proteinosis; PAS, periodic acid-Schiff; pLN, peripheral lymph node; P-Luc, promoter-luciferase; PNA, peanut agglutinin; SIRS, systemic inflammatory response syndrome.

www.jimmunol.org/cgi/doi/10.4049/jimmunol.1102991

the maximal production of cytokines and cell expansion, because Runx1-transduced CD4$^+$ cells show a reduction in both IL-2 production and cell proliferation in vitro upon stimulation (19). Conversely, deleting Runx1 in naive CD4$^+$ T cells induces IL-2 production and cell proliferation, as noted using *Runx1$^{f/f}$CD4^{cre}* mice (19, 20). These observations led to the investigation of the potential role of Runx1 in maintaining quiescence of naive CD4$^+$ T cells. However, mice with Runx1-deficient T cells suffer from lymphopenia, which is likely due to the enhancement of cell apoptosis and impairment of cell homeostasis (19, 20). The occurrence of lymphopenia in *Runx1$^{f/f}$CD4^{cre}* mice makes it difficult to analyze the role of Runx1 in quiescence control by using these mice. In *CBFβ$^{f/f}$CD4^{cre}* mice, CBFβ is deleted in CD4$^+$ T cells, and mice develop asthma-like symptoms (21). However, the CBFβ cofactor is shared by three members of the Runx family; thus, *CBFβ$^{f/f}$CD4^{cre}* mice are not suitable for analyzing the specific function of Runx1 in CD4$^+$ T cells.

In the current study, *Runx1$^{f/f}$CD4^{cre}* mice were crossed with Bcl2-transgenic (*Bcl2^{tg}*) mice to improve the survival and total number of Runx1-deleted CD4$^+$ T cells. Strikingly, Runx1 deficiency caused spontaneous hyperactivation of CD4$^+$ T cells, their preferential homing to the lungs, and the increased production of cytokines, such as IL-17 and IL-21, from cells. Mice eventually developed a fatal autoimmune lung disease and severe systemic inflammation. Our observations indicate that Runx1 plays an essential role in repressing cytokine expression and, thereby, maintaining CD4$^+$ T cells in a quiescence stage.

Materials and Methods

Mice

Conditional Runx1-knockout (*Runx1$^{fl/fl}$*) mice were prepared, as previously described (22). To delete Runx1 specifically in CD4$^+$ T cells, *Runx1$^{fl/fl}$* mice were crossed with CD4-Cre-tg mice (23). Bcl2 expression in T lymphocytes was enforced by crossing mice with *Bcl2^{tg}* mice (B6.Cg-Tg [BCL2]25Wehi/J) (24) to generate *Runx1$^{f/f}$;CD4-Cre-tg;Bcl2^{tg}* mice (denoted as *Runx1$^{-/-}$Bcl2^{tg}*). CD4$^+$ T cell-deficient mice (B6.129S2-Cd4tm1Mak) (25) and C57BL/6 mice were from The Jackson Laboratory and CLEA, respectively. Ly5.1$^+$ (CD45.1)-C57BL/6 mice were as described previously (26). All mice were kept in a pathogen-free environment and handled in accordance with the Regulations for Animal Experiments and Related Activities at Tohoku University.

Flow cytometry analyses

Cell suspensions were prepared from spleens, lymph nodes, lungs, or thymuses of mice, and 1×10^6 cells were stained with the following Abs: FITC-B220, FITC-heat stable Ag, PE-TCRβ, PE-CXCR3, PE-CCR5, allophycocyanin-B220, and PECy7-CD8a (BioLegend, San Diego, CA); FITC-CD69, FITC-Fas, PE-CD21, PE-CD40L, PE–Gr-1, PE-CD103, allophycocyanin–Mac-1, and biotin–syndecan-1 (BD Pharmingen, San Jose, CA); FITC-CCR9, FITC-CD23, FITC-NK1.1, PE-CD11a, PE-CD44, PECy5-CD62L, PE–Cy7–IgM, and allophycocyanin-CD4 (eBiosciences, San Diego, CA); PE-Thy1 (Cell Laboratory, Fullerton, CA); and biotin-c–peanut agglutinin (PNA) (Biomeda, Burlingame, CA). Cells stained with biotin-conjugated Abs were subjected to secondary incubation with streptavidin-PE (BD Pharmingen). For intracellular staining of cytokines, CD4$^+$ T cells were isolated from splenocytes using anti-mouse CD4 Magnetic Particles-DM (BD Biosciences). The purity of isolated cells was >93%. Cells were incubated in RPMI 1640/10% FBS for 4 h in the presence of 200 ng/ml PMA, 1 μM ionomycin, and 2 μM monensin. Intracellular staining was performed using a Fix and Perm kit (Invitrogen, Carlsbad, CA). The Abs used were FITC–IFN-γ, PE–IL-17 (BD Biosciences), and PE–IL-21 (R&D Systems, Minneapolis, MN). For the detection of nuclear Foxp3, a PE-Foxp3 Ab and staining buffer set (eBiosciences) were used. Apoptosis was assayed using the Mebcyto Apoptosis kit (MBL, Nagoya, Japan). TCR polyclonality was analyzed with a Mouse Vβ TCR Screening kit (BD Biosciences). Flow cytometry analyses were carried out in a Cytomics FC500 and analyzed with CXP analysis software.

Bronchoalveolar lavage cells and cytokine analyses

Mouse lungs were lavaged three times with 700 μl PBS, and the recovered bronchoalveolar lavage fluid (BALF) was centrifuged at 300 × *g* for 5 min. For the pellets, the number of cells was counted by a hemocytometer, and cell types were identified by flow cytometry analyses of cell surface markers. For the supernatants, the amount of cytokines was measured using a Cytometric Bead Array Mouse Th1/Th2 Cytokine Kit (BD Biosciences, San Jose, CA). A 50-μl volume was incubated with mixed capture beads for 2 h in the dark, washed, and processed for flow cytometry analyses. Mean fluorescence intensities were measured. The concentrations of each cytokine were extrapolated by the equation of each standard curve ($R^2 \geq 0.99$).

Adoptive transfer and mixed bone marrow chimera experiments

CD4$^+$ T cells were collected from spleens of 16–24-wk-old donor mice using anti-mouse CD4 Magnetic Particles-DM (BD Biosciences), and 3×10^6 cells were injected into tail veins of 8–12-wk-old CD4$^+$ T cell-deficient mice. Recipient mice were sacrificed for histological analyses after 5 or 25 wk of injection. In chimera experiments, cells were collected from bone marrow (BM) of congenic Ly5.1$^+$ (CD45.1)-C57BL/6 and *Runx1$^{-/-}$Bcl2^{tg}* (CD45.2$^+$) mice and depleted of CD4$^+$ T cells using anti-mouse CD4 Magnetic Particles-DM. A 1:1 mixture of each genotype of cells (total 5×10^6) was injected i.v. into tail veins of C57BL/6 mice that had been lethally irradiated (9 Gy). Recipient mice were given 2 mg/ml G418 (Sigma, St. Louis, MO) in drinking water for the first 2 wk and were sacrificed for analyses at 8 wk after transplantation.

Histology

Mouse tissues were fixed in 3.7% (w/v) paraformaldehyde in PBS and kept at 4°C. Tissues were weighed after they were drained on a tissue tower. For analysis of lung tissues, inflation with formalin was performed before excision. Paraffin sections were prepared and stained with H&E, Elastica-Masson (EM), and periodic acid-Schiff (PAS), according to standard procedures. In certain cases, paraffin sections were counterstained by an anti-surfactant protein A Ab (Millipore, Bedford, MA). Lung histology was scored as follows: grade 0, normal lung; grade 1, mild/limited peribronchovascular infiltration of lymphocytes; grade 2, severe/frequent peribronchovascular infiltration of lymphocytes; and grade 3, severe/frequent peribronchovascular infiltration of lymphocytes with massive accumulation of exudate in the alveoli. Cryostat sections were prepared, blocked with 5% (w/v) BSA in PBS, and stained with anti-mouse IgG (H+L) F(ab′)$_2$-488 (Cell Signaling, Danvers, MA), FITC–anti-CD4 (eBiosciences), FITC–anti-IgD, FITC–anti-B220, PE–anti-CD4 (all from BioLegend), or biotin-c–PNA (Biomeda), followed by FITC-streptavidin for 1 h in the dark and viewed through a Zeiss LSM5 PASCAL confocal microscope. In certain cases, frozen sections were stained with Sudan III.

ELISA of serum Ig

A 96-well plate was coated with mouse serum (1000-fold diluted) at 37°C for 2 h, blocked with 1% (w/v) BSA in PBS, and incubated with goat anti-mouse IgM/IgG1/IgG2a HRP-labeled Abs (2000-fold dilution) (Bethyl, Montgomery, TX) for 1 h. Color was developed by tetramethylbenzidine peroxidase substrate (Bethyl), stopped by 1 M HCl, and analyzed on a SpectraMax M2e plate reader. Anti-dsDNA Abs in sera were measured using an anti-mouse dsDNA ELISA kit (Shibayagi, Gunma, Japan).

Immunoblotting and RT-PCR

CD4$^+$ T or CD8$^+$ T cells were isolated from splenocytes using the respective anti-mouse Magnetic Particles-DM (BD Biosciences), and 1×10^6 cells were lysed in SDS sample buffer and sonicated. The lysate was centrifuged, and the supernatant was mixed with SDS sample buffer. Denatured samples were then run on SDS-polyacrylamide gels and transferred onto membranes. Filters were incubated with Abs, followed by the AP-conjugated secondary Ab (at 1:4000 dilution), and immune complexes were detected using NBT/BCIP substrate (Promega, Madison, WI). The *Pan*-Runx Ab was as described previously (27). Bcl2 (100) and β-actin Abs were from Santa Cruz Biotechnology (Santa Cruz, CA) and Sigma, respectively. For RT-PCR analysis, RNA was extracted from isolated cells using TRIzol reagent and reverse transcribed using SSRT II (Invitrogen, Carlsbad, CA). The primers used were described previously (19).

Plasmid construction

Expression vectors of Runx1-hemagglutinin or dominant-negative Runt-hemagglutinin were constructed by inserting the respective sequences into a pCAGGSNeo plasmid. To synthesize a reporter driven by the mouse IL-21 promoter-luciferase (P-Luc), the mouse genomic sequence was amplified using the primers 5′-GAAGATCTGTCAGACAAACCAGGTGAGGTG-3′ and 5′-CCCAAGCTTCTGAGTCTCCAGGAGCTGATGA-3′. Underlined

sequences represent restriction enzyme sites for BglII and HindIII. The PCR products containing a promoter region from −398 to +43 were digested and ligated into the BglII and HindIII sites of the pGL3 reporter. To insert a conserved noncoding sequence (CNS) region, a mouse genomic sequence was amplified using the primers 5′-AAAGGTACCGGATAGTCACAGGG-AGTTTGTTCT-3′ and 5′-AAAAGATCTGAATCCTCTCAGGGACAA-TCAG-3′. Underlined sequences represent KpnI and BglII sites. The PCR products containing a CNS region from +2890 to +3437 were digested and ligated into the KpnI and BglII sites of P-Luc to generate a CNS+P-Luc reporter. For mutagenesis, the Runx sites at locations +3114 and +3162 were mutated from TGTGGT to TCTAAG using a PCR-amplification method. Primers used for the construct were m1: 5′-AAGCCGGTTC-TAAGCAAAAAGAAG-3′ and 5′-CTTCTTTTTGCTTAGAACCGGCTT-3′; m2: 5′-AACATGAACATCTAAGTTTCAAGG-3′ and 5′-CCTTGAA-ACTTAGATGTTCATGTT-3′; and m1&2: 5′-CGGTTCTAAGCAAAAA-GAAGAGAAAAGAAAAAAACTTCAACAAACATGAACATCTAAGT-TTC-3′ and 5′-GAAACTTAGATGTTCATGTTTGTTGAAGTTTTTTTC-TTTTCTCTTCTTTTTGCTTAGAACCG-3′. The sequences of mutated Runx sites are underlined.

Luciferase reporter and chromatin immunoprecipitation assay

Jurkat cells were transfected with a total of 500 ng plasmid DNA using FuGENE HD (Roche, Indianapolis, IN). After 24 h, cells were stimulated with 200 ng/ml PMA and 1 μM ionomycin for 6 h before harvest. Luciferase activity was measured by the Dual-Luciferase Reporter Assay System (Promega), as described (28). pRL-TK (5 ng) was included in each transfection as a normalization control for transfection efficiency. A chromatin immunoprecipitation (ChIP) assay was performed, as described previously (19). Briefly, $CD4^+$ T cells were purified from splenocytes of C57BL/6 mice, fixed, sonicated, and precipitated with control IgG or an anti-Runx1 Ab (Abcam). The following primers were used for amplification of the IL-21 CNS region: for the Runx site at +3114 (CNS-1): 5′-AGGTAGCTTGCCTGTCACTAGGGCAAAGTG-3′ and 5′-TTTTTCC-AGTAAGTTAAGCCGGTTGTGGTC-3′ and for the Runx site at +3162 (CNS-2): 5′-TTTTTGACCACAACCGGCTTAACTTACTGG-3′ and 5′-TACGACCCCTCCCCAAGCTTCTTTGGAACG-3′. A ChIP library was constructed from the precipitate using TruSeq RNA Sample Prep Kit v2 (Illumina, San Diego, CA). Quantitative PCR was performed using SsoAdvanced SYBR Green Supermix (Bio-Rad, Hercules, CA) in a real-time PCR CFX96 machine.

Statistical analysis

All statistical data were evaluated using an unpaired two-tailed Student *t* test and were considered significant if $p < 0.05$.

Results

Generation of mice harboring a Runx1-deleted $CD4^+$ T cell population

To examine the function of Runx1 in naive $CD4^+$ T cells, Runx1 expression in $CD4^+$ T cells was disrupted by breeding *Runx1$^{f/f}$* mice, in which the Runx1 exon 5 is flanked by the loxP sites (details of targeting vector were described previously) (22), with *CD4-Cre-tg* mice (23) to yield *Runx1$^{f/f}$;CD4-Cre-tg* mice (hereafter referred to as *Runx1$^{-/-}$*). Immunoblot analyses of splenocytes were used to confirm that Runx1 protein amounts were reduced by ~90% in *Runx1$^{-/-}$* $CD4^+$ T cells (Fig. 1A, note that in a $CD8^+$ subset, Runx3, not Runx1, was dominant; therefore the reduction of Runx1 was not apparent). In *Runx1$^{-/-}$* mice, spleens were of a smaller size and weight (Fig. 1B) and contained significantly lower numbers of $CD4^+$ T cells compared with control littermates ($0.41 \pm 0.22 \times 10^7$ versus $2.0 \pm 0.47 \times 10^7$; Fig. 1C).

Because *Runx1$^{-/-}$* mice suffered from a severe reduction in the $CD4^+$ T cell population, this population was boosted by crossing them with *Bcl2^{tg}* mice (24) to yield *Runx1$^{f/f}$;CD4-Cre-tg;Bcl2^{tg}* mice (hereafter referred to as *Runx1$^{-/-}$Bcl2^{tg}*). The expression of transduced Bcl2 protein in T cells from control or *Runx1$^{-/-}$Bcl2^{tg}* spleens was confirmed by immunoblot analyses (Fig. 1A). Bcl2 did not affect the efficiency of the Runx1 deletion in *Runx1$^{-/-}$Bcl2^{tg}* $CD4^+$ T cells. Spleens with a *Bcl2^{tg}* background displayed an increase in size and weight (Fig. 1B) due to the expansion of the TCR-β^+, $CD4^+$, and $CD8^+$ T populations (Fig. 1C). This is consistent with a previous report showing an increased lymphocyte number in *Bcl2^{tg}* mice due to enhanced cell viability and resistance to apoptosis (24). As a consequence, *Runx1$^{-/-}$Bcl2^{tg}* spleens contained an increased number ($2.0 \pm 1.4 \times 10^7$ versus $0.41 \pm 0.22 \times 10^7$) and percentage of $CD4^+$ T cells compared with those of *Runx1$^{-/-}$* mice without a *Bcl2^{tg}* background (Fig. 1C, data not shown).

Splenocytes were then stained with annexin V and propidium iodide (Fig. 1D). The percentages of apoptotic (annexin V+) cells among the $CD4^+$ fraction were 2.8-fold higher in *Runx1$^{-/-}$* mice than in *Runx1$^{+/+}$* mice ($18.7 \pm 4.4\%$ versus $6.8 \pm 2.3\%$). The presence of the *Bcl2* transgene significantly reduced the percentages of apoptotic $CD4^+$ T splenocytes to $7.6 \pm 4.5\%$ in *Runx1$^{-/-}$Bcl2^{tg}* mice. Results similar to those above were also obtained by staining cells with anti-ssDNA Ab (data not shown). This indicates that the reduction of Runx1 in $CD4^+$ T cells induced apoptosis, which can be prevented by Bcl2 transduction. Given that *Runx1$^{-/-}$Bcl2^{tg}* mice contained substantial numbers of Runx1-deleted peripheral $CD4^+$ T cells, these mice were used to explore the possible role of Runx1 in maintaining the quiescence status of T cells. *Runx1$^{+/-}$Bcl2^{tg}* mice were used as controls.

Runx1$^{-/-}$Bcl2^{tg} *mice develop severe lung inflammation*

The development and growth of *Runx1$^{-/-}Bcl2^{tg}$* mice were apparently normal, and no recognizable phenotypes were detected during young adulthood. However, after >28 wk, *Runx1$^{-/-}Bcl2^{tg}$* mice inevitably showed tachypnea, took a hunched posture (data not shown), and suffered from general weakness and loss of body weight (Fig. 2A). More than 70% of *Runx1$^{-/-}Bcl2^{tg}$* mice died between 28 and 36 wk of age (Fig. 2B). None of them had a life span > 56 wk, whereas all of the control mice survived this observation period.

To explore the cause(s) of death, young (16–24-wk-old) and aged (28–36-wk-old) *Runx1$^{-/-}Bcl2^{tg}$* mice, together with age-matched control mice, were sacrificed, and the internal organs were examined. Macroscopically, the lungs from *Runx1$^{-/-}Bcl2^{tg}$* mice were substantially large, diffusively red, and 2.3-fold heavier than were those from control mice (0.61 ± 0.07 g versus 0.26 ± 0.02 g) (Fig. 2C). Histological sections of the lung were stained by H&E, EM, and PAS (Fig. 2D). With all three staining methods, the infiltration and accumulation of lymphoid cells into peribronchovascular interstitial regions were observed in the lungs from both young and aged *Runx1$^{-/-}Bcl2^{tg}$* mice. This infiltration was not seen in control *Runx1$^{+/-}Bcl2^{tg}$* mice. In accordance with lymphoid infiltration in the lungs, peripheral lymph nodes (pLN) and lung-draining mediastinal lymph nodes (mLN) from *Runx1$^{-/-}Bcl2^{tg}$* mice were also markedly enlarged compared with those from control littermates (data not shown).

In the lungs of aged *Runx1$^{-/-}Bcl2^{tg}$* mice (Fig. 2D), many alveolar spaces were filled with exudates that contained eosinophilic granular materials and a vast amount of immune cells (predominantly neutrophils and foamy macrophages.). Fig. 2E is a higher magnification of such alveolar spaces. Exudates were stained positive for eosin and surfactant protein A, whereas alveolar macrophages were stained positive for surfactant protein A and Sudan III, indicating their engulfing activity. Based on these hallmarks, the pathology seen in the *Runx1$^{-/-}Bcl2^{tg}$* lungs was considered similar to pulmonary alveolar proteinosis (PAP) in humans (29). Note that this PAP-like pathology was detected focally in the young *Runx1$^{-/-}Bcl2^{tg}$* lungs as well.

The disease score of mice was determined by observing histological sections (Fig. 2F), as described in *Materials and Methods*.

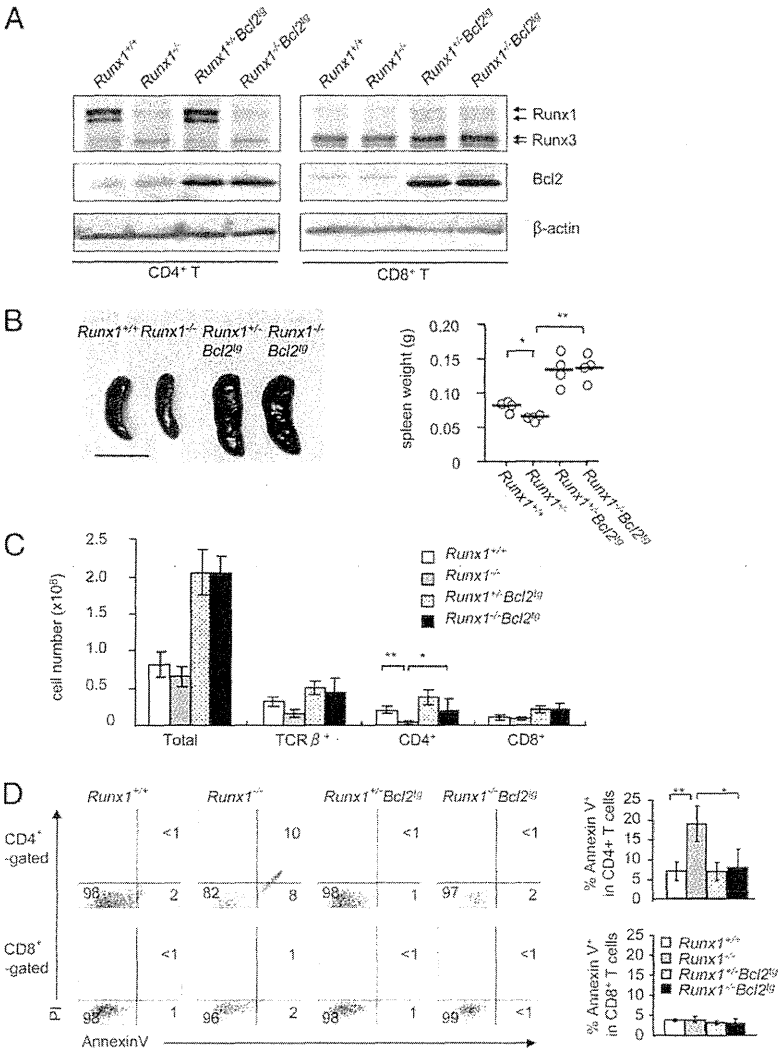

FIGURE 1. Overexpression of *Bcl2* rescues apoptotic *Runx1*-deleted CD4$^+$ T cells. (**A**) Confirmation of *Runx1* deletion and *Bcl2* transgene expression by immunoblot analyses. CD4$^+$ and CD8$^+$ T cells were purified from spleens of 8–12-wk-old *Runx1*$^{+/+}$, *Runx1*$^{-/-}$, *Runx1*$^{+/-}$*Bcl2*^{tg}, or *Runx1*$^{-/-}$*Bcl2*^{tg} mice. Lysates were prepared and processed. β-actin served as a loading control. (**B**) A representative photograph of spleens from 8–12-wk-old mice (*left panel*). Scale bar, 1 cm. Spleen weights of 8–12-wk-old mice (*right panel*; n = 4). *p = 0.01, **p = 0.0003. (**C**) The number of CD4$^+$ T cells increased after *Bcl2* transgene expression. Cell numbers of total, TCRβ$^+$, CD4$^+$, or CD8$^+$ splenocytes from 8–12-wk-old mice (n = 4). *p = 0.046, **p = 0.0004. (**D**) The percentages of apoptotic cells were reduced in the presence of *Bcl2* transgene expression. Flow cytometry analyses of splenocytes derived from 8–12-wk-old mice. Bar graphs show mean (± SD) percentages of annexin V$^+$ cells in the CD4$^+$- or CD8$^+$-gated populations derived from each mouse (n = 4). *p = 0.013, **p = 0.0012.

Lungs from young *Runx1*$^{-/-}$*Bcl2*^{tg} mice scored between 1 and 2, whereas those from aged mice scored up to 3, reflecting the more severe pathology in aged mice. In contrast, lungs from age-matched control mice showed no pathological phenotype and scored 0.

To monitor airway-residing immune cells, BALF was recovered, and the cells in it were analyzed (Fig. 3A, 3B). Strikingly, in aged (but not young) *Runx1*$^{-/-}$*Bcl2*^{tg} mice, ~5-fold greater numbers of BALF cells were detected compared with control littermates. BALF cells from *Runx1*$^{-/-}$*Bcl2*^{tg} mice were composed predominantly of Gr-1$^+$Mac-1$^+$ granulocytes and, to lesser degrees, TCR-β$^+$ T cells, B220$^+$ B cells, and Gr-1$^-$Mac-1$^+$ macrophages. Also, the levels of proinflammatory cytokines, such as IFN-γ and TNF, were ~3-fold higher in BALF from aged *Runx1*$^{-/-}$*Bcl2*^{tg} mice compared with control mice (Fig. 3C). This suggests the occurrence of a cytokine storm in the lungs of aged *Runx1*$^{-/-}$*Bcl2*^{tg} mice.

Systemic inflammation in aged Runx1$^{-/-}$Bcl2^{tg} *mice*

Organs other than the lungs were examined next. In young *Runx1*$^{-/-}$*Bcl2*^{tg} mice, tissues from the kidneys, liver, pancreas, or the digestive tract exhibited normal histology (data not shown). In contrast, aged *Runx1*$^{-/-}$*Bcl2*^{tg} mice developed a wasting disease of various organs, including muscles. For example, in the liver of aged mice (Fig. 4A), hepatocytes were atrophic, whereas sinusoids were enlarged and contained immune cells. Glycogenesis appeared insufficient, probably due to ischemia. The hemocyte count of peripheral blood (Table I) revealed slightly increased numbers of RBC and increased hemoglobin concentration and hematocrit percentage, suggesting compensatory erythrocytosis, whereas the numbers of WBC were decreased to less than half. In addition, the percentages of Gr-1^{med}Mac-1$^+$ monocytes were remarkably increased in peripheral blood (monocytosis in Fig. 4B), suggesting the presence of a chronic systemic inflammation in aged *Runx1*$^{-/-}$*Bcl2*^{tg} mice. Consistently, the levels of IFN-γ and TNF were elevated in sera from aged *Runx1*$^{-/-}$*Bcl2*^{tg} mice compared with control mice (Fig. 4C).

Altogether, the phenotypes described above suggest that active inflammation, such as lymphocyte infiltration, was initially limited to local areas in the lung of young *Runx1*$^{-/-}$*Bcl2*^{tg} mice. Subsequently, chronic and exacerbated immune responses resulted in SIRS in the aged *Runx1*$^{-/-}$*Bcl2*^{tg} mice, as exemplified by symptoms such as wasting disease, organ dysfunction, and lethality. In addition, aged *Runx1*$^{-/-}$*Bcl2*^{tg} mice developed a pathology similar to PAP.

Runx1-deleted CD4$^+$ T cells traffic to the lung and initiate lung inflammation

To examine whether the lung-infiltrating cells in *Runx1*$^{-/-}$*Bcl2*^{tg} mice were Runx1-deleted CD4$^+$ T cells, immunofluorescent de-

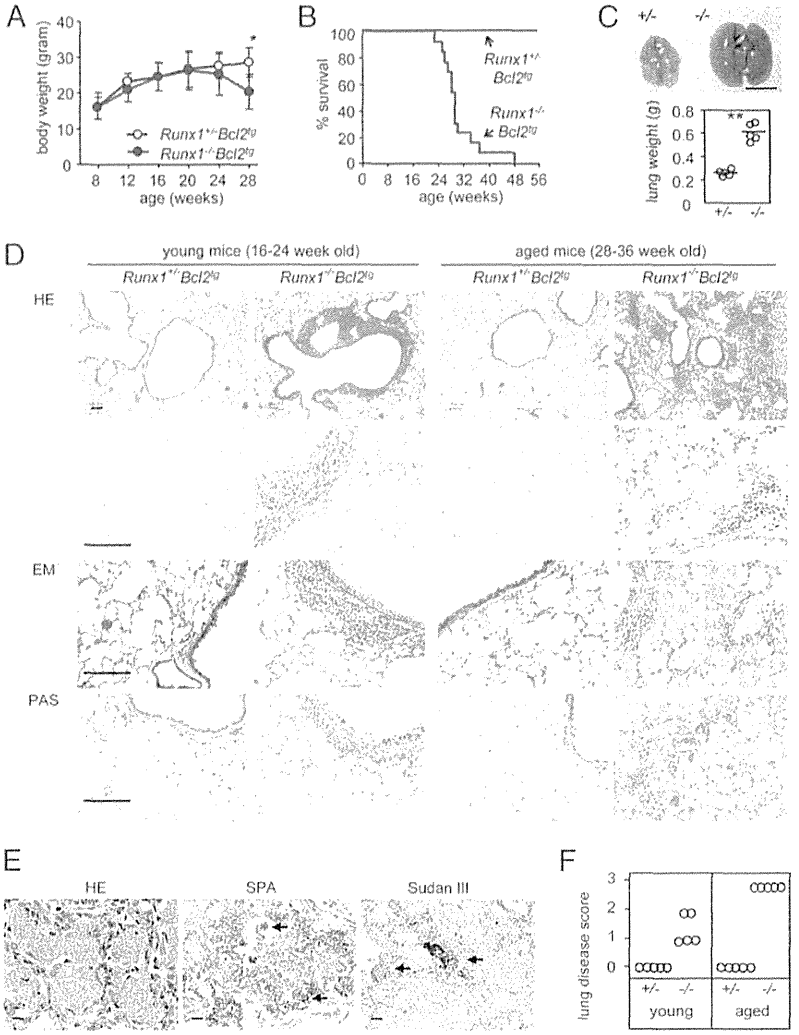

FIGURE 2. Mice harboring *Runx1*-deficient T cells develop lethal lung inflammation. **(A)** Weight loss in aged $Runx1^{-/-}Bcl2^{tg}$ mice. Body weights of $Runx1^{-/-}Bcl2^{tg}$ and control mice between 8 and 28 wk of age. Shown are mean ± SD (n = 6–8 mice per each age group). *p = 0.0038. **(B)** Reduced survival of $Runx1^{-/-}Bcl2^{tg}$ mice. Survival rate percentages of control and $Runx1^{-/-}Bcl2^{tg}$ mice within 1 y of age (n = 13). **(C)** A representative photograph of lungs derived from >28-wk-old control ($^{+/-}$) or $Runx1^{-/-}Bcl2^{tg}$ ($^{-/-}$) mice (*top panel*). The lungs from $Runx1^{-/-}Bcl2^{tg}$ mice became enlarged and diffusively red. Weights of lungs from >28-wk-old control ($^{+/-}$) and $Runx1^{-/-}Bcl2^{tg}$ ($^{-/-}$) mice (n = 5–6; *bottom panel*). **p = 0.000003. **(D)** Histology of lung tissue sections of control and $Runx1^{-/-}Bcl2^{tg}$ mice. Tissues were stained with H&E, EM, or PAS (n = 5). Scale bars, 100 μm. **(E)** PAP-like histology in the lungs of aged $Runx1^{-/-}Bcl2^{tg}$ mice. Lung sections were stained with H&E or Sudan III or counterstained with an Ab to surfactant protein A (SPA). n = 3. Scale bars, 10 μm. **(F)** Lung disease scores of control ($^{+/-}$) and $Runx1^{-/-}Bcl2^{tg}$ ($^{-/-}$) mice at the indicated ages (n = 5).

tection of the CD4 Ag was performed in frozen lung sections (Fig. 5A). As expected, $CD4^+$ T cells concentrated in the peribronchovascular regions of $Runx1^{-/-}Bcl2^{tg}$ (but not control) lungs.

The mechanism by which the Runx1-deleted $CD4^+$ T cells preferentially targeted the lungs was investigated by assessing whether Runx1 deletion caused deregulation of the expression of integrins. $CD4^+$-gated fractions from $Runx1^{-/-}Bcl2^{tg}$ splenocytes showed reduced expression of CD62L, a marker of homing to lymphoid organs (Fig. 5B). Expression of the gastrointestinal homing markers CD103 and CCR9 was subtle in $Runx1^{-/-}Bcl2^{tg}$ cells; in contrast, CD11a expression was substantially enhanced. Runx1 was reported to regulate CD11a expression by binding to a Runx site in the promoter (30). CD11a is a subunit of LFA-1, which interacts with ICAM1 expressed on the vessel wall in bronchial mucosa (31). We also examined chemokine receptors, such as CXCR3 and CCR5, which are important for lung infiltration (32, 33). Interestingly, the cell surface level of CXCR3 was increased, whereas CCR5 was not markedly changed in $Runx1^{-/-}Bcl2^{tg}$ $CD4^+$ T cells. Therefore, increased expression of CD11a and CXCR3 might cause the retention of Runx1-deficient $CD4^+$ cells in the lung.

The detection of various types of immune cells in the aged $Runx1^{-/-}Bcl2^{tg}$ lungs suggested that the infiltrating Runx1-deleted $CD4^+$ T cells may be responsible for the subsequent inflammation in the lungs. To address this possibility, $Runx1^{-/-}Bcl2^{tg}$ $CD4^+$ T cells were adoptively and intravenously transferred into $CD4^+$ T cell-deficient mice, and the lungs of these recipient mice were examined. Interestingly, recipient mice injected with $Runx1^{-/-}Bcl2^{tg}$ $CD4^+$ T cells showed lung phenotypes similar to those of donor mice, and disease scores were 1–2 at 5 wk and 2–3 at 25 wk postinjection (Fig. 5C, 5D). Infiltration of lymphocytes to the peribronchovascular region of recipient mice lungs strongly suggested that the Runx1-deleted $CD4^+$ T cells were capable of homing to the lungs, activating an immune response and causing inflammation.

Runx1-deleted $CD4^+$ T cells are hyperactivated

To better understand the mechanisms underlying the aggressive immune responses of $Runx1^{-/-}Bcl2^{tg}$ mice, spleens, pLN, and mLN were excised from nonimmunized control mice and $Runx1^{-/-}Bcl2^{tg}$ mice and examined by flow cytometry (Fig. 6A). As seen in the summary of Fig. 6B, naive cells ($CD44^{lo}CD62L^{hi}$) constituted only a small proportion (13 ± 9.3%) of the $CD4^+$-gated population in $Runx1^{-/-}Bcl2^{tg}$ lymphatic tissues compared with control tissues (49 ± 14%). Meanwhile, the majority of $CD4^+$-gated cells exhibited an active/memory phenotype ($CD44^{hi}$) in $Runx1^{-/-}Bcl2^{tg}$ tissues compared with control tissues (76 ± 13% versus 41 ± 10%). In addition, a 1.5–2.0-fold increase in the $CD69^+$ and $CD40L^+$ fractions was observed in the $CD4^+$-gated

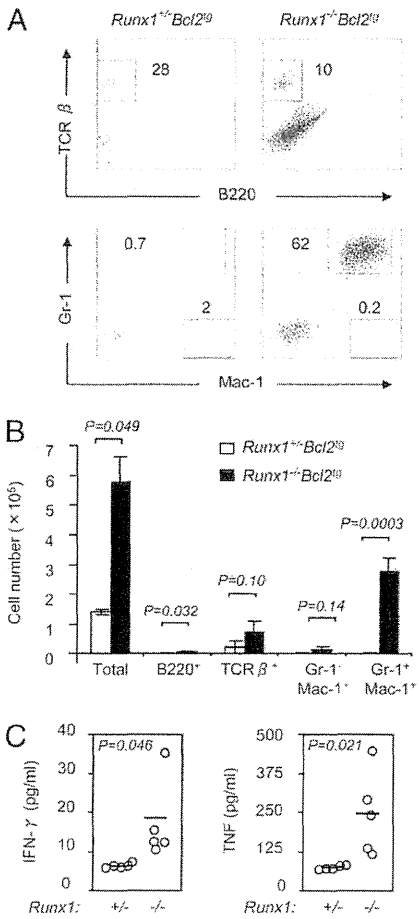

FIGURE 3. Increase in immune cells and proinflammatory cytokines in BALF of *Runx1*$^{-/-}$*Bcl2*^{tg} mice. (**A**) Flow cytometry analyses of cells in BALF. Representative results from three independent experiments are shown. (**B**) Bar graphs show mean (± SD) cell counts in BALF prepared from 24–32-wk-old control and *Runx1*$^{-/-}$*Bcl2*^{tg} mice (n = 3). Immune cells, including lymphocytes (B220$^+$ and TCRβ$^+$) and neutrophils (Gr-1$^+$Mac-1$^+$), were increased in *Runx1*$^{-/-}$*Bcl2*^{tg} mice. The B220$^+$ fraction constituted a small population in BALF but was increased in *Runx1*$^{-/-}$*Bcl2*^{tg} mice (1329 ± 1681 versus 7725 ± 106). (**C**) Amounts of proinflammatory cytokines IFN-γ and TNF in BALF derived from >28-wk-old control ($^{+/-}$) or *Runx1*$^{-/-}$*Bcl2*^{tg} ($^{-/-}$) mice (n = 5).

Runx1$^{-/-}$*Bcl2*^{tg} tissues compared with control tissues (Fig. 6C, 6D). These findings indicated the continuous activation of Runx1-deleted CD4$^+$ T cells.

One possible explanation for the presence of autoactivated T cells is the escape of immature, self-reactive thymocytes into the periphery. Examination of thymocyte differentiation (Supplemental Fig. 1) revealed that the percentage of CD4-single positive cells was reduced to half in *Runx1*$^{-/-}$*Bcl2*^{tg} mice (2.4% compared with 4.4% in the control). However, the percentage of HSA^{low} TCR-β$^+$ mature cells in the CD4$^+$ gate did not differ significantly between control and *Runx1*$^{-/-}$*Bcl2*^{tg} thymuses (37% versus 33%). Furthermore, most of the CD4$^+$ cells in the two spleen genotypes belonged to a mature stage (89% versus 88%). Therefore, despite the delay in early thymocyte development in *Runx1*$^{-/-}$*Bcl2*^{tg} mice, CD4$^+$ cells appeared to be released into the periphery as fully mature T cells.

Another explanation for the presence of autoactivated CD4$^+$ T cells could be the expansion of a particular T cell clone capable of recognizing a specific Ag. To address this possibility, the expression of TCR V region β-chains (Vβ) in control and *Runx1*$^{-/-}$*Bcl2*^{tg} CD4$^+$ T cells was analyzed (Supplemental Fig. 2). Similar distribution patterns of TCR Vβ were observed in the two cell genotypes, confirming the polyclonality of cells.

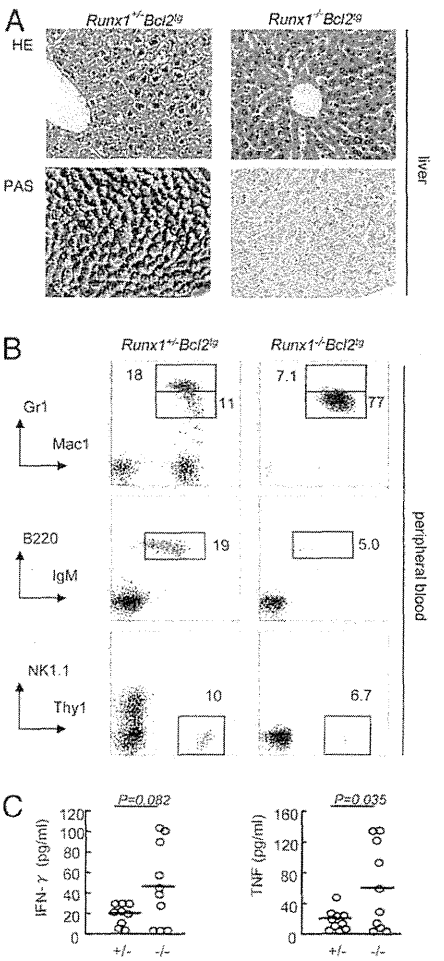

FIGURE 4. Aged *Runx1*$^{-/-}$*Bcl2*^{tg} mice develop SIRS. (**A**) Glycogenesis insufficiency in livers of aged *Runx1*$^{-/-}$*Bcl2*^{tg} mice. Liver sections from 28–36-wk-old control and *Runx1*$^{-/-}$*Bcl2*^{tg} mice were stained. H&E staining showed atrophy of hepatocytes, as well as enlargement of sinusiods. PAS-positive materials were abundant in the periphery of hepatocytes of control mice but were not detected in the *Runx1*$^{-/-}$*Bcl2*^{tg} hepatocytes, suggesting poor glycogenesis. Original magnification ×40. (**B**) Monocytosis in aged *Runx1*$^{-/-}$*Bcl2*^{tg} mice. Peripheral blood was collected from aged (>28-wk-old) control and *Runx1*$^{-/-}$*Bcl2*^{tg} mice and analyzed by flow cytometry staining. The percentage of monocytes (Gr-1^{int}Mac-1^{hi}) was dramatically increased in *Runx1*$^{-/-}$*Bcl2*^{tg} mice, indicating a presence of chronic inflammation and suggesting an increased demand for, for example, phagocytotic activity in the inflamed tissues. Percentages of other lineages, including B (B220$^+$IgM$^+$), NK (NK1.1$^+$), or T (Thy1$^+$) cells, were relatively reduced as the result of an increase in monocytes. Data are representative of two independent experiments. Note that monocytosis was not observed in the peripheral blood of young *Runx1*$^{-/-}$*Bcl2*^{tg} mice. (**C**) Elevated levels of proinflammatory cytokines in sera from aged *Runx1*$^{-/-}$*Bcl2*^{tg} mice. Sera were collected from aged (>28-wk-old) control ($^{+/-}$) and *Runx1*$^{-/-}$*Bcl2*^{tg} ($^{-/-}$) mice (n = 10 for each genotype). Amounts of IFN-γ (*left panel*) and TNF (*right panel*) were measured by cytokine bead array, using 5-fold diluted sera. The p values were evaluated by the unpaired Student t test.

A third possible explanation for autoactivated T cells is the dysfunction of Treg. As seen in Supplemental Fig. 3A, the percentage of Foxp3$^+$ cells among the CD4$^+$ subset was increased in *Runx1*$^{-/-}$*Bcl2*^{tg} spleens compared with control spleens (37%

Table I. Hemocyte counts

	Runx1$^{+/-}$ *Bcl2*^{tg}		*Runx1*$^{-/-}$ *Bcl2*^{tg}	
	Young	Aged	Young	Aged
WBC ($\times 10^2/\mu l$)	233 ± 90	223 ± 43	230 ± 54	94 ± 70
RBC ($\times 10^4/\mu l$)	993 ± 84	985 ± 28	993 ± 54	1150 ± 171
HGB (g/dl)	15 ± 1	15 ± 1	15 ± 1	16 ± 2
HCT (%)	48 ± 4	48 ± 1	48 ± 3	51 ± 6
MCV (fl)	48 ± 1	49 ± 1	48 ± 2	45 ± 3
MCH (pg)	15 ± 0	15 ± 1	15 ± 1	14 ± 1
MCHC (g/dl)	31 ± 1	32 ± 1	31 ± 1	32 ± 1
PLT ($\times 10^4/\mu l$)	97 ± 25	95 ± 4	90 ± 15	107 ± 40

Peripheral blood cell numbers from young (16–24-wk-old) and aged (>28-wk-old) control and *Runx1*$^{-/-}$*Bcl2*^{tg} mice were counted using Celltac-α machine (NihonKoden, Tokyo, Japan). Aged *Runx1*$^{-/-}$*Bcl2*^{tg} mice showed decreased numbers of WBC and increased numbers/values for RBC, hemoglobin (HGB), and hematocrit (HCT). Decreased WBC appears in accordance with the occurrence of SIRS in aged *Runx1*$^{-/-}$*Bcl2*^{tg} mice. In contrast, erythrocytosis suggests that the host's compensatory response mechanisms to a decreased oxygen supply to organs (hypoxia) is caused by severe lung inflammation and respiratory failure in aged *Runx1*$^{-/-}$*Bcl2*^{tg} mice. MCV, Mean corpuscular volume; MCH, mean corpuscular hemoglobin; MCHC, mean corpuscular hemoglobin concentration; PLT, platelet.

versus 14%). In support of this observation, increased *CTLA4* and *CD25* mRNA expression was detected in CD4$^+$ T cells purified from *Runx1*$^{-/-}$*Bcl2*^{tg} spleens (Supplemental Fig. 3B). An increase in Foxp3$^+$ Treg might function to circumvent the robust immune responses in *Runx1*$^{-/-}$*Bcl2*^{tg} mice. Therefore, the autoactivation of CD4$^+$ T cells seen in *Runx1*$^{-/-}$*Bcl2*^{tg} mice likely was not due to an impairment of thymocytes or Treg differentiation but rather was due to the dysregulation of intrinsic transcriptional control.

To further confirm an intrinsic process of CD4$^+$ T cell activation, we performed chimera experiments by transplanting BM cells from CD45.1$^+$-C57BL/6 and *Runx1*$^{-/-}$*Bcl2*^{tg} (CD45.1$^-$) mice into irradiated C57BL/6 recipient mice. Reconstituted cells in spleen, pLN, mLN, and lung of recipient mice were examined after 8 wk (Fig. 6E). CD4$^+$ T cells derived from *Runx1*$^{-/-}$*Bcl2*^{tg} BM contained a substantially greater percentage of memory/effector cells and fewer naive cells compared with the corresponding cells derived from wild-type BM. Notably, CD4$^+$ T cells from *Runx1*$^{-/-}$*Bcl2*^{tg} lung contained the highest percentage of effector/memory cells (84 ± 2%). The observations strongly suggest that Runx1 deficiency-mediated hyperactivation of CD4$^+$ T cells reflects a cell-intrinsic process.

Runx1-deleted CD4$^+$ T cells produce elevated levels of cytokines

To examine whether the Runx1-deleted CD4$^+$ T cells that showed an activated phenotype produced cytokines, the mRNA levels of cytokines were measured by RT-PCR (Fig. 7A). In the *Runx1*$^{-/-}$*Bcl2*^{tg} CD4$^+$ splenocytes, *IL-21* mRNA levels were 5-fold higher than in control cells (2.0 ± 0.09 versus 0.41 ± 0.24 folds). Similarly, the levels of proinflammatory cytokine *IL-17A* mRNA were also increased (1.9 ± 0.18 versus 0.29 ± 0.11). Consistent with our previous study (19), Runx1 deletion caused increased expression of the T cell growth factor cytokine *IL-2* (2.4 ± 0.68 versus 0.31 ± 0.38), which suggested actively dividing Runx1-deleted CD4$^+$ T cells. Furthermore, *IL-10* expression levels were increased (2.1 ± 0.45 versus 0.08 ± 0.05), which was in accordance with the increased percentage of Treg in *Runx1*$^{-/-}$*Bcl2*^{tg} mice. These data suggested that the Runx1 deletion in naive CD4$^+$ T cells led to spontaneous hyperactivation of cells, as reflected in the transcriptional induction of a wide range of cytokines. No significant increase in the *IFN-γ* mRNA level was detected in *Runx1*$^{-/-}$*Bcl2*^{tg} cells.

The expression of cytokines was next examined by flow cytometry after in vitro stimulation of CD4$^+$ T cells with PMA plus

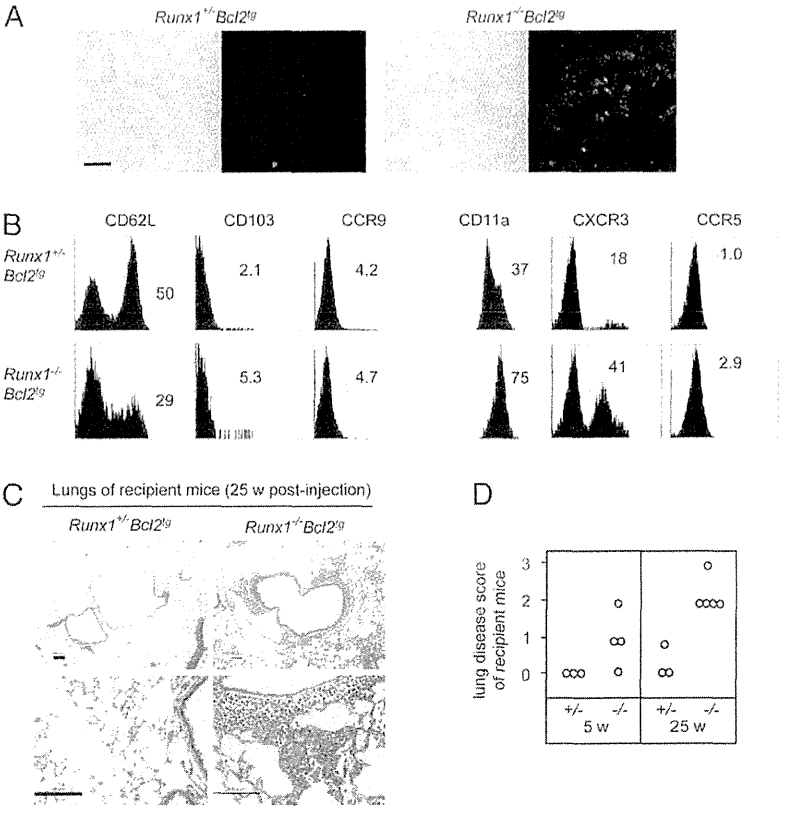

FIGURE 5. *Runx1*-deficient CD4$^+$ T cells infiltrate into the lung and initiate lung inflammation. (**A**) Accumulation of CD4$^+$ T cells in the lung interstitial region. Immunofluorescence staining of lung sections from >28-wk-old control and *Runx1*$^{-/-}$*Bcl2*^{tg} mice with an FITC-CD4 Ab. Scale bar, 100 μm. Data are representative of three independent experiments (n = 3). (**B**) Expression profiles of integrins and chemokine receptors in *Runx1*-deficient CD4$^+$ T cells. Surface expression of CD62L, CD103, CCR9, CD11a, CXCR3, and CCR5 in CD4$^+$ T-gated cells from control or *Runx1*$^{-/-}$*Bcl2*^{tg} spleens. Data are representative of three independent experiments. (**C** and **D**) Adoptive-transfer experiments of *Runx1*-deficient CD4$^+$ T cells. Control or *Runx1*$^{-/-}$*Bcl2*^{tg} CD4$^+$ T cells were isolated and injected into CD4$^+$ T cell-deficient mice. At 5 or 25 wk postinjection, recipient mice were sacrificed for lung examination. (C) Representative histology of lung sections from recipient mice at 25 wk postinjection. Sections were stained with H&E; scale bars, 100 μm. (D) Scoring of lung disease (n = 3–5).

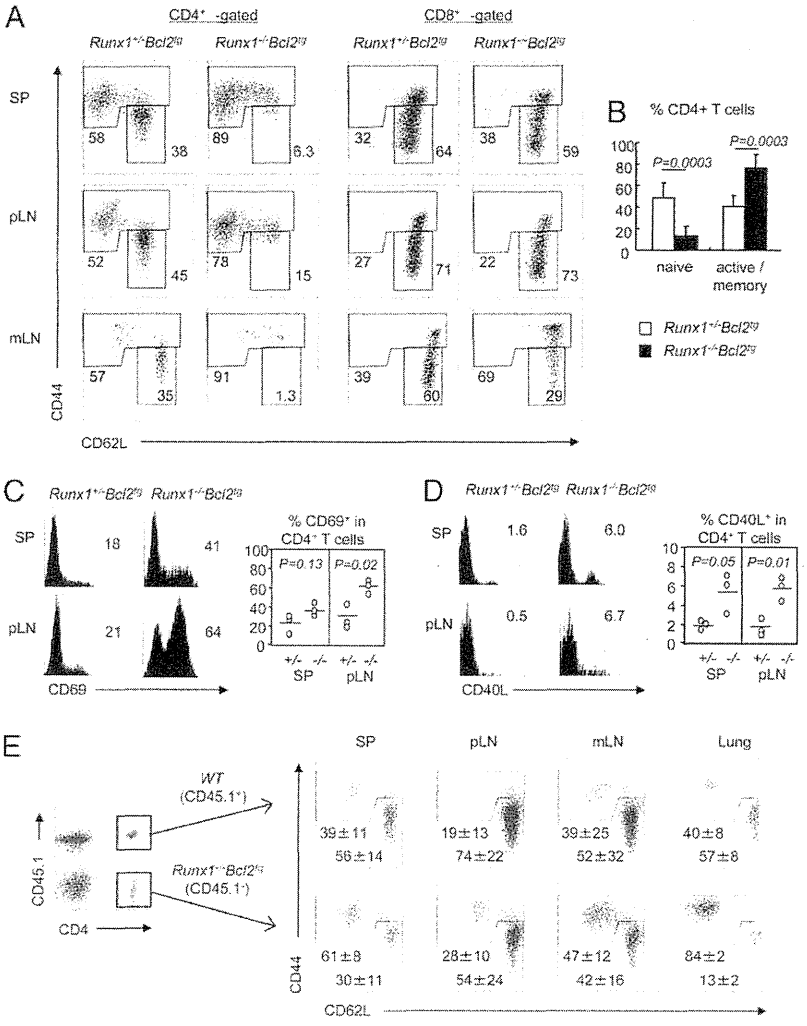

FIGURE 6. *Runx1*-deficient CD4$^+$ T cells are hyperactivated. (**A**) *Runx1*-deleted CD4$^+$ T cells gained active/memory phenotypes. Flow cytometry analyses of CD44 and CD62L expression on CD4$^+$ or CD8$^+$ T cells derived from spleens (SP), pLN, and mLN of 24–32-wk-old control and *Runx1*$^{-/-}$*Bcl2*^{tg} mice. The percentages of naive (CD62L^{hi}CD44^{lo}) and active/memory (CD62L^{lo} CD44^{hi} or CD62L^{hi}CD44^{hi}) fractions among the CD4$^+$- or CD8$^+$ T-gated cells are indicated. Data are representative of four independent experiments. (**B**) Bar graphs show the percentages (mean ± SD) of naive and active/memory cells among the CD4$^+$ fractions from control or *Runx1*$^{-/-}$*Bcl2*^{tg} mice. The average percentage was calculated from SP, pLN, and mLN (n = 4). (**C** and **D**) Surface expression of the activation markers CD69 and CD40L in CD4$^+$ T cells from spleens and pLN of 24–32-wk-old control or *Runx1*$^{-/-}$*Bcl2*^{tg} mice. Data are representative of three independent experiments (n = 3). (**E**) Flow cytometry analyses of naive versus active/memory phenotypes in CD4$^+$ T cells reconstituted by mixed-BM chimera experiment. C57BL/6 mice were lethally irradiated and transplanted by a mixture of wild-type (WT; CD45.1$^+$) and *Runx1*$^{-/-}$*Bcl2*^{tg} (CD45.1$^-$) BM cells. After 8 wk, spleen (SP), pLN, mLN, and lung were prepared and analyzed. Numbers shown are mean ± SD from two independent experiments (n = 4).

ionomycin (Fig. 7B). The percentages of IL-21$^+$ and IL-17$^+$ cells were several-fold higher in the spleens and pLN of *Runx1*$^{-/-}$*Bcl2*^{tg} mice compared with controls, suggesting that the *Runx1*$^{-/-}$*Bcl2*^{tg} CD4$^+$ T cells were more or less committed to differentiate into cytokine-producing effector T cells.

Runx1 suppresses the transcription of IL-21

Runx1 is reported to regulate the transcription of *IL-2*, *IL-4*, and *IL-17* (12, 13, 19). The role of Runx1 in *IL-21* expression is not known, although the role of IL-21 in both inflammation and the formation of IgG-secreting plasma cells is well established. This prompted an examination of the transcriptional regulation of IL-21 by Runx1. Transcription of *IL-21* is controlled by two DNase-hypersensitive sites (HS) designated promoter (P)/HS1 and HS2 (34). Using Vista comparative genomic tools, an additional CNS was identified in intron 2 (Fig. 8A). This ~500-bp region of CNS was 99% identical between human and mouse, suggesting that it has a potentially important function. The P, HS2, and CNS sequences from different species were aligned and searched for Runx binding sites. Notably, two Runx binding sites were identified in the CNS region (Supplemental Fig. 4) but not in the P or HS2 regions. To test the functional significance of the CNS region, the P and CNS regions of *IL-21* were ligated to a luciferase reporter (Fig. 8B). When transfected into Jurkat cells, both P-Luc and CNS+P-Luc plasmids showed only minimal basal activity. However, PMA plus ionomycin treatment of cells markedly induced P activity (27 ± 3-fold), as previously reported (34, 35). The addition of the CNS region further enhanced the reporter activity (42 ± 4-fold), indicating positive regulation by a response element in the CNS.

To examine whether Runx1 is involved in the regulation of CNS activity, the reporters were cotransfected with a Runx1-expressing vector, which was induced by PMA plus ionomycin (Fig. 8C). Runx1 reduced CNS+P-Luc activity to 50%, whereas it did not affect P-Luc activity. As a control, the cotransfection of Runt, a dominant-negative form of Runx1, did not reduce the CNS+P-Luc activity. In the case of CNS+SV40P-Luc, in which the *IL-21* promoter was replaced by the SV40 promoter, Runx1 reduced the activity to 30%, confirming the negative role of the CNS region in *IL-21* regulation (Fig. 8D). Mutations were then introduced into two Runx sites in the CNS, individually or simultaneously (Fig. 8E). Mutations of the Runx site at +3114 (m1), +3162 (m2), or both sites (m1&m2) partially or completely abolished the Runx1-mediated reduction in CNS activity.

ChIP assay was carried out to examine Runx1 binding to the *IL-21* CNS region. Lysates prepared from unstimulated CD4$^+$ T cells from C57BL/6 mice were immunoprecipitated with a Runx1 Ab. Sequences spanning each Runx site in the CNS, but not the promoter, were recovered as enriched (Fig. 8F). To further confirm the Runx1 binding, a concentrated DNA library was prepared and processed for quantitative real-time PCR. The CNS-1 and CNS-2 regions were successfully enriched (Fig. 8G). The results collec-

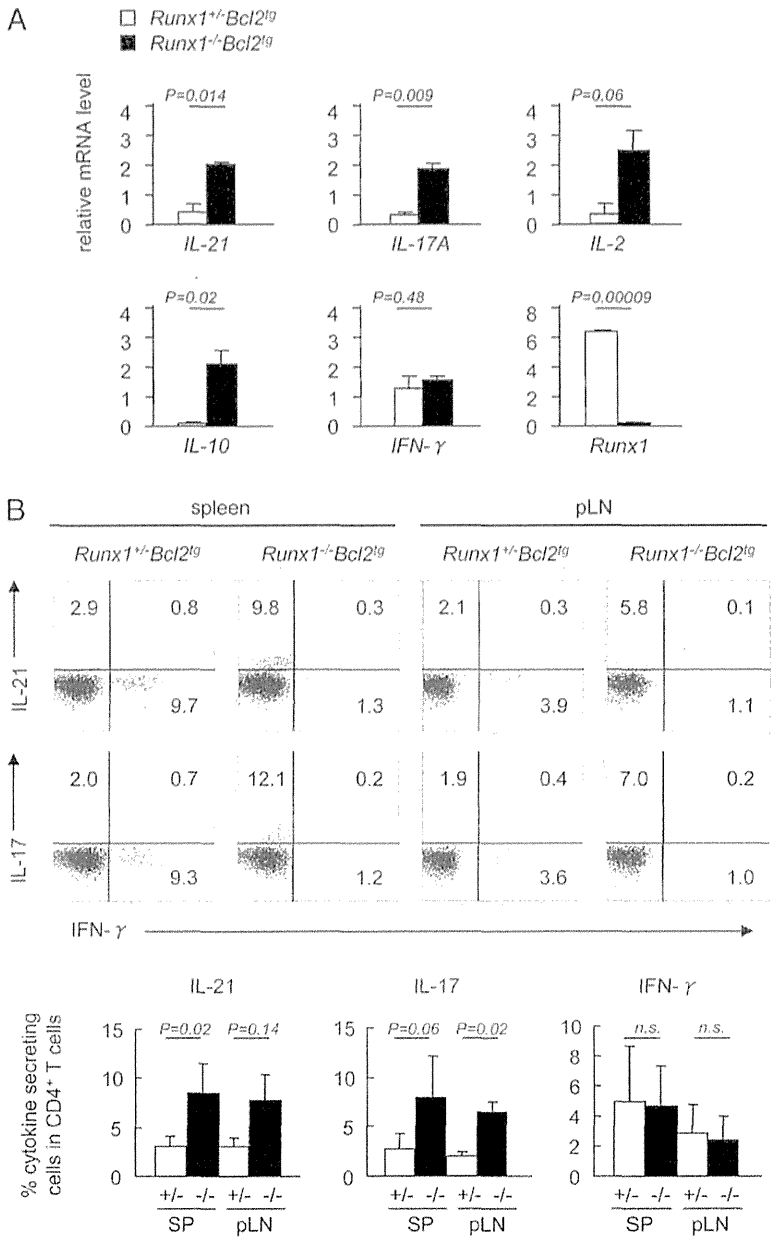

FIGURE 7. Enhanced expression of IL in *Runx1*-deficient $CD4^+$ T cells. (**A**) Relative amounts of *IL* transcripts compared with those of *β-actin*. $CD4^+$ T cells were purified from 24–32-wk-old control and $Runx1^{-/-}Bcl2^{tg}$ spleens. RNA was prepared and processed for semiquantitative RT-PCR analyses. Band intensities were compared and quantified, using *β-actin* as a control. Bar graphs are mean ± SD from two independent experiments. (**B**) $CD4^+$ T cells were purified from the spleens or pLN of 24–32-wk-old control and $Runx1^{-/-}Bcl2^{tg}$ mice. Cells were stimulated in vitro with PMA plus ionomycin and processed for intracellular staining of indicated IL and flow cytometry analyses. Representative data from three independent experiments are shown. Bar graphs show the percentages of cytokine-positive $CD4^+$ T cells in spleen or pLN from the control ($^{+/-}$) and $Runx1^{-/-}Bcl2^{tg}$ ($^{-/-}$) mice. Mean ± SD from three independent experiments is shown.

tively indicated that Runx1, if present, functions negatively to repress *IL-21* expression through binding to the CNS region.

Germinal center formation and Ab secretion in $Runx1^{-/-}Bcl2^{tg}$ *mice*

Increased expression of IL-21 was observed in Runx1-deleted $CD4^+$ T cells. An increase in IL-21 expression is associated with the development of inflammatory and autoimmune diseases in mice (36). For example, IL-21 can induce the differentiation of activated $CD4^+$ T cells into proinflammatory Th17 cells (37–39). In addition, IL-21 is important in promoting the formation of the germinal center (GC) and in the differentiation of B cells into Ig-secreting plasma cells (40–43).

Immunofluorescence was used to examine the effect of Runx1 deletion on GC formation, and the results showed that T ($CD4^+$) and B ($B220^+$) cell zones in white pulps were disrupted in $Runx1^{-/-}Bcl2^{tg}$ spleens (Fig. 9A). Furthermore, in white pulps of $Runx1^{-/-}Bcl2^{tg}$ spleens, IgD^+ naive B cells were not detected in the follicle region; PNA (a GC marker)-positive cells were detected instead (Fig. 9B). Analysis by flow cytometry (Fig. 9C) revealed a 2-fold increase in PNA^+Fas^{hi} cells (both are GC markers) in the $Runx1^{-/-}Bcl2^{tg}$-derived $CD4^+$ fraction compared with the control (28 ± 10% versus 14 ± 6%), whereas a 1.5-fold increase in PNA^+Fas^{hi} cells was detected in the $Runx1^{-/-}Bcl2^{tg}$-derived $B220^+$ fractions (13 ± 9.6% versus 8.2 ± 4.1%). These observations indicate that GC formation is accelerated spontaneously in Runx1-deleted spleens.

Because GC formation is associated with the expansion of B cells and Ig class switching, B cell phenotypes were examined further. A 2-fold increase in syndecan-1^+B220^{med} Ig-secreting plasma cells was observed in $Runx1^{-/-}Bcl2^{tg}$ spleens compared with controls (3.7 ± 0.6% versus 1.8 ± 0.4%; Fig. 9D).

The possible development of hyperimmunoglobulinemia in $Runx1^{-/-}Bcl2^{tg}$ mice was examined by measuring titers of Ig isotypes in sera. IgM and IgG2a levels (but not IgG1) were moderately increased in $Runx1^{-/-}Bcl2^{tg}$ mice compared with

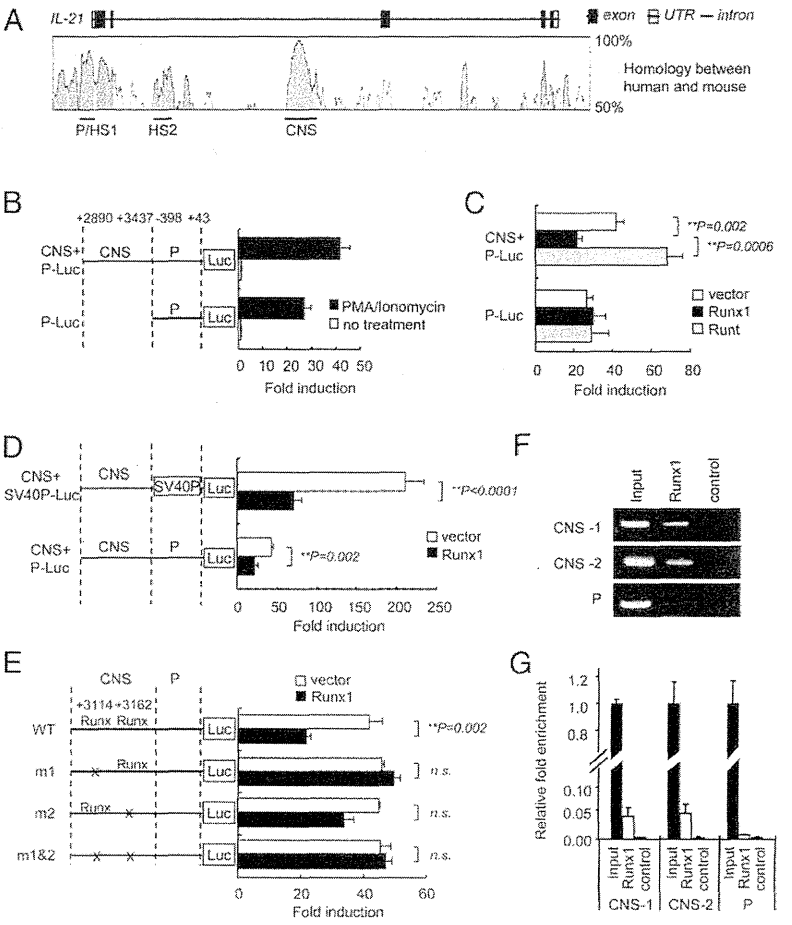

FIGURE 8. Runx1 controls *IL-21* transcription as revealed by reporter assays. (**A**) Homology of *IL-21* gene sequences between humans and mice, as detected by Vista browser. Location of the *IL-21* promoter (P), DNase-hypersensitive sites (HS1 or HS2), and CNS are indicated. (**B**) Jurkat cells were transfected with *IL-21* CNS+P-Luc or P-Luc reporters and treated or not with PMA plus ionomycin. (**C–E**) Jurkat cells were cotransfected with an *IL-21* reporter and an empty, Runx1- or Runt-expressing vector and stimulated with PMA plus ionomycin. (E) Mutations introduced into the Runx sites at +3114 or +3162 are indicated by "x." In (B)–(E), the reporter activities recovered are shown as fold induction (mean ± SD). In one experiment, samples were run in triplicate; representative results of three independent experiments are shown. (**F**) Runx1 binds to the *IL-21* CNS region inside cells. $CD4^+$ T cells from C57BL/6 mice were subjected to ChIP with anti-Runx1 Ab or control IgG, and the precipitates were processed for PCR. (**G**) Relative amounts of input, anti-Runx1 ChIP, or control in a concentrated library, as quantified by real-time PCR. In (F) and (G), the precipitated DNA was amplified with primers to CNS-1 (recognizing the Runx-site at +3114), CNS-2 (recognizing the Runx site at +3162), and negative control P (promoter harboring no Runx site). n.s., not significant.

control mice (Fig. 9E). Interestingly, the titers of anti-dsDNA Ab were also higher in *Runx1*$^{-/-}$*Bcl2*^{tg} mice than in control mice. However, the titer of anti-dsDNA in *Runx1*$^{-/-}$*Bcl2*^{tg} mice was a few-fold lower than in aged *MPL*$^{lpr/lpr}$ mice (data not shown). Finally, frozen sections of lung were stained by fluorescein-tagged anti-IgG (Fig. 9F). Some interstitial lymphoid cells were positive for IgG staining, an indication of plasma cells. Altogether, the above observations suggest that plasma cell-associated humoral responses, including autoantibodies, might be involved in lung pathogenesis.

Discussion

Runx1$^{-/-}$*Bcl2*^{tg} mice generated in this study developed severe lung disease in the absence of Ag challenge. Mixed pathological phenotypes were observed, such as lymphoid infiltration into peribronchovascular interstitial regions and granulocyte-, foamy macrophage-, and surfactant protein A-containing exudates into alveolar spaces. Also, high titers of proinflammatory cytokines in BALF suggested the existence of severe inflammatory responses in the lungs. Additionally, the mice suffered from systemic inflammatory responses and died at ~6–7 mo of age.

It is noteworthy that some of the pathology seen in *Runx1*$^{-/-}$*Bcl2*^{tg} lungs resembled PAP in humans. In 90% of cases of human PAP, the emergence of neutralizing autoantibodies against GM-CSF in sera appears to be responsible for the pathogenesis (44). In mouse models, PAP is generated by targeting GM-CSF, and mice exhibit pulmonary lymphoid hyperplasia, as well as alveolar proteinosis (45, 46). In humans and mice that lack GM-CSF signaling, the accumulation of exudates in alveolar spaces is attributed to a dysfunction of alveolar macrophages in clearing surfactant proteins (29). In our *Runx1*$^{-/-}$*Bcl2*^{tg} mice, anti–GM-CSF autoantibodies were not detected in sera (data not shown), and alveolar macrophages were found to be positive for surfactant protein A and Sudan III, an indication of cellular engulfing activity. Although there are no reports linking T lymphocyte abnormality to PAP, a possible cytokine storm in the lung might somehow cause macrophage dysfunction and the consequent failure to digest the incorporated materials.

It must be noted that although GM-CSF–null mice suffer from lung disease, the mice are apparently healthy and have a normal life span. In contrast, *Runx1*$^{-/-}$*Bcl2*^{tg} mice died before they reached 6–7 mo old, suggesting a much more severe and complicated pathogenesis in our mice. At a terminal stage in *Runx1*$^{-/-}$*Bcl2*^{tg} mice, systemic inflammation developed, probably due to the leakage of cytokines into the circulation. As signs of SIRS, various complications, such as monocytosis, blood coagulation, muscle wasting syndrome, and liver failure, commonly occur (10). Indeed, at least some of the above signs were confirmed in older *Runx1*$^{-/-}$*Bcl2*^{tg} mice. In addition, the chronic reactivity of $CD4^+$ T cells is reported to drive autoimmunity and destructive inflammation (47). Thus, the characteristic pathology of *Runx1*$^{-/-}$*Bcl2*^{tg} mice would be the development of lung-localized inflammation as well as systemic inflammation.

Circulating T lymphocytes, while preserving their ability to fight invading pathogens, are maintained in a quiescent stage and prevented from unnecessary autoactivation. In early studies, quiescence was considered a default stage of mature T cells before encountering a cognate Ag. Subsequently, increasing numbers of

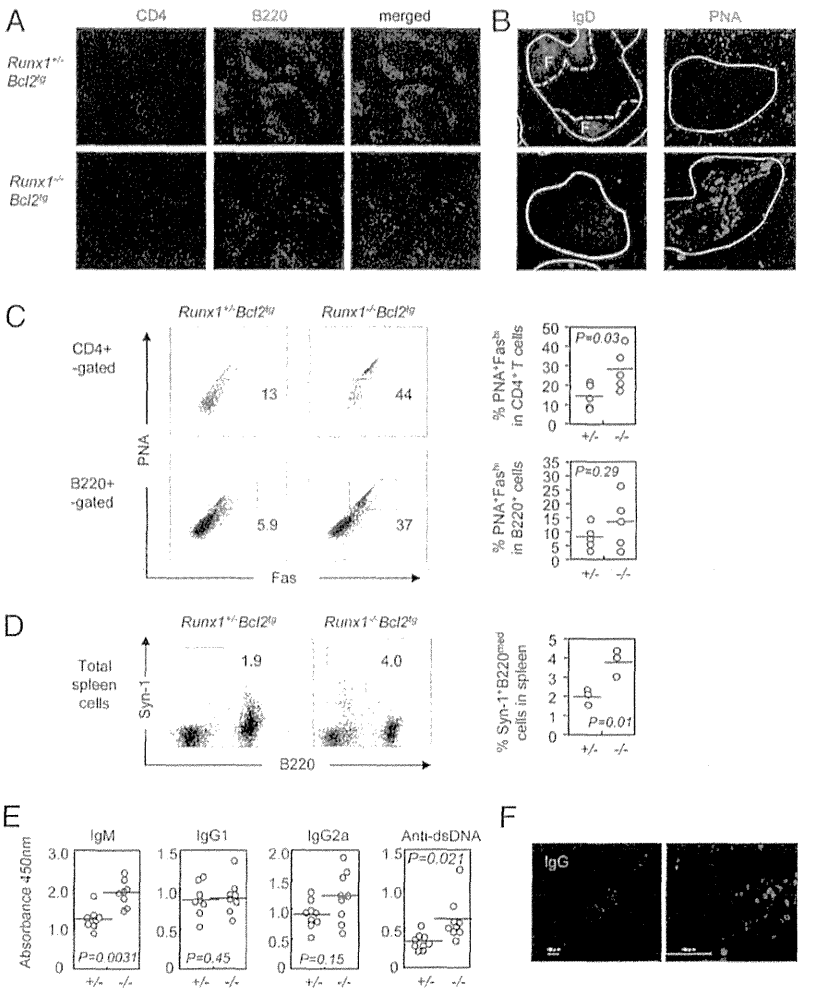

FIGURE 9. Enhancement of GC formation, plasma cell mobilization, and serum Ig levels in *Runx1*$^{-/-}$*Bcl2*^{tg} mice. (**A** and **B**) Immunofluorescence staining of spleens from 24–32-wk-old control and *Runx1*$^{-/-}$*Bcl2*^{tg} mice with anti-CD4, anti-B220, anti-IgD, or anti-PNA Abs. Representative images from two independent experiments are shown. White pulps and follicle areas (F) are indicated by solid and dashed white lines, respectively. Original magnification ×10. Flow cytometry analyses of PNA^{hi}Fas^{+} GC cells in CD4^{+} and B220^{+} splenocytes (**C**) and Syn-1^{hi}B220^{med} plasma B cells in splenocytes (**D**). Control ($^{+/-}$) and *Runx1*$^{-/-}$*Bcl2*^{tg} ($^{-/-}$) 24–32-wk-old mice were used. Data are representative of five (C) or three (D) independent experiments. (**E**) Levels of Ig subtypes in sera. ELISA analyses of IgM, IgG1, IgG2a, and anti-dsDNA in sera from 24–32-wk-old control ($^{+/-}$) and *Runx1*$^{-/-}$*Bcl2*^{tg} ($^{-/-}$) mice (n = 8–9). (**F**) Immunofluorescence staining of IgG on frozen lung sections from 24–32-wk-old *Runx1*$^{-/-}$*Bcl2*^{tg} mice. Scale bar, 100 μm. Data are representative of three independent experiments (n = 3).

studies suggested that the maintenance of quiescence in T cells required the activity of transcription factors, such as Klf2, Tob, Foxo, Slfn2, Tsc1, and Foxp1 (2–8). However, the thus-far reported quiescence-related molecules are also involved in the regulation of cell homeostasis, cell survival, and/or cell trafficking, and their targeting often results in a lymphopenic situation in mice. Therefore, the loss of cell quiescence seen in targeted mice might be due to the induction of cell proliferation to compensate for lymphopenia, and a quiescence control mechanism remains a controversial issue. We avoided this complexity by protecting cells from apoptosis with the use of the Bcl2 transgene and observed that *Runx1*$^{-/-}$*Bcl2*^{tg} CD4^{+} T cells exhibited hyperactivated phenotypes, as judged by the expression of activation markers (CD62L^{lo}CD44^{hi}CD69^{+}), the lung-homing integrin molecule CD11a, and various cytokines. The present results suggest that Runx1 may function as a guardian of naive CD4^{+} T cells in their quiescence stage.

Then how does a Runx1 deficiency lead to the disruption of cell quiescence? The spontaneous expression of various cytokines in naive *Runx1*$^{-/-}$*Bcl2*^{tg} CD4^{+} T cells suggests that Runx1 might contribute to quiescence by intrinsically suppressing the expression of various cytokines in resting T cells. Regulation of cytokine genes, such as *IL-2*, *IL-4*, or *IL-17*, by Runx1 was reported (12, 13, 19). In this study, we explored the regulation of *IL-21* transcription by Runx1 because IL-21 is closely associated with both inflammatory (37–39) and autoimmune diseases (41, 48). We found that the ectopic expression of Runx1 suppressed the PMA plus ionomycin-induced CNS activity of *IL-21*. Multiple Runx and NFAT binding sites were identified in the CNS region. One possibility is that Runx1 binding to the CNS suppresses *IL-21* transcription by masking the NFAT binding sites. Conversely, the lack of Runx1, as in the case of *Runx1*$^{-/-}$*Bcl2*^{tg} CD4^{+} T cells, is likely to cause an induction of *IL-21* transcription through a derepression mechanism.

IL-21 plays important roles in inflammation through its ability to induce IL-17 expression (37–39), whereas IL-17, in turn, mediates immunopathogenesis in experimental hypersensitivity pneumonitis and bronchiolitis obliterans syndrome [e.g. (49, 50)]. In a mouse model of experimental autoimmune encephalitis, IL-21 deficiency slowed disease progression as the result of a secondary effect of IL-17 reduction (38). In Runx1-deficient CD4^{+} T cells, expression of both IL-17 and IL-21 were increased. Augmentation of IL-21 might exacerbate lung inflammation indirectly through the enhancement of IL-17 expression in *Runx1*$^{-/-}$*Bcl2*^{tg} mice. However, an IL-17–independent role for IL-21, if any, in the inflammatory responses seen in *Runx1*$^{-/-}$*Bcl2*^{tg} lungs remains to be elucidated.

The known, direct effects of IL-21 are the enhancement of GC formation and the generation of IgG-secreting plasma cells (40–43). As seen in *Runx1*$^{-/-}$*Bcl2*^{tg} mice, an increased percentage of B cells became plasma cells in the spleen GC. IgG^{+} plasma cells were detected in the lung, although it is not clear whether they produced autoantibodies that contributed to pathogenesis in the *Runx1*$^{-/-}$*Bcl2*^{tg} lungs. Levels of IgM, IgG2a, and anti-dsDNA Ab

in sera were moderately increased, indicating the mobilization of humoral immune responses. It is possible that Abs produced by IgG^+ plasma cells might cooperate with other immune cells and exacerbate the localized immune responses in the lung, as well as systemic inflammation.

In conclusion, the current study suggests a novel role for the Runx1 transcription factor in maintaining the quiescent stage of mature $CD4^+$ T cells in peripheral lymphoid tissues. Deletion of Runx1 in naive $CD4^+$ T cells caused spontaneous cellular activation and cytokine production that eventually led to a catastrophic autoimmune inflammatory disease. The pathology seen in *Runx1*$^{-/-}$*Bcl2*^{tg} lungs was similar to that of human PAP. This study also implies a therapeutic potential of the Runx1 molecule for the suppression of inflammatory disease mediated by hyperactivated $CD4^+$ T cells.

Acknowledgments

We thank I. Taniuchi (RIKEN, Yokohama, Japan) for CD4-Cre-tg mice and Y. Yoshikai and H. Yamada (Kyushu University, Kyushu, Japan) for *Bcl2*^{tg} mice. We thank M. Kuji for secretarial assistance.

Disclosures

The authors have no financial conflicts of interest.

References

1. Yusuf, I., and D. A. Fruman. 2003. Regulation of quiescence in lymphocytes. *Trends Immunol.* 24: 380–386.
2. Berger, M., P. Krebs, K. Crozat, X. Li, B. A. Croker, O. M. Siggs, D. Popkin, X. Du, B. R. Lawson, and A. N. Theofilopoulos, et al. 2010. An Slfn2 mutation causes lymphoid and myeloid immunodeficiency due to loss of immune cell quiescence. *Nat. Immunol.* 11: 335–343.
3. Buckley, A. F., C. T. Kuo, and J. M. Leiden. 2001. Transcription factor LKLF is sufficient to program T cell quiescence via a c-Myc–dependent pathway. *Nat. Immunol.* 2: 698–704.
4. Feng, X., H. Wang, H. Takata, T. J. Day, J. Willen, and H. Hu. 2011. Transcription factor Foxp1 exerts essential cell-intrinsic regulation of the quiescence of naive T cells. *Nat. Immunol.* 12: 544–550.
5. Kuo, C. T., M. L. Veselits, and J. M. Leiden. 1997. LKLF: A transcriptional regulator of single-positive T cell quiescence and survival. *Science* 277: 1986–1990.
6. Medema, R. H., G. J. Kops, J. L. Bos, and B. M. Burgering. 2000. AFX-like Forkhead transcription factors mediate cell-cycle regulation by Ras and PKB through p27kip1. *Nature* 404: 782–787.
7. Tzachanis, D., G. J. Freeman, N. Hirano, A. A. van Puijenbroek, M. W. Delfs, A. Berezovskaya, L. M. Nadler, and V. A. Boussiotis. 2001. Tob is a negative regulator of activation that is expressed in anergic and quiescent T cells. *Nat. Immunol.* 2: 1174–1182.
8. Yang, K., G. Neale, D. R. Green, W. He, and H. Chi. 2011. The tumor suppressor Tsc1 enforces quiescence of naive T cells to promote immune homeostasis and function. *Nat. Immunol.* 12: 888–897.
9. Tzachanis, D., E. M. Lafuente, L. Li, and V. A. Boussiotis. 2004. Intrinsic and extrinsic regulation of T lymphocyte quiescence. *Leuk. Lymphoma* 45: 1959–1967.
10. Davies, M. G., and P. O. Hagen. 1997. Systemic inflammatory response syndrome. *Br. J. Surg.* 84: 920–935.
11. Wong, W. F., K. Kohu, T. Chiba, T. Sato, and M. Satake. 2011. Interplay of transcription factors in T-cell differentiation and function: the role of Runx. *Immunology* 132: 157–164.
12. Komine, O., K. Hayashi, W. Natsume, T. Watanabe, Y. Seki, N. Seki, R. Yagi, W. Sukzuki, H. Tamauchi, K. Hozumi, et al. 2003. The Runx1 transcription factor inhibits the differentiation of naive CD4+ T cells into the Th2 lineage by repressing GATA3 expression. *J. Exp. Med.* 198: 51–61.
13. Zhang, F., G. Meng, and W. Strober. 2008. Interactions among the transcription factors Runx1, RORgammat and Foxp3 regulate the differentiation of interleukin 17-producing T cells. *Nat. Immunol.* 9: 1297–1306.
14. Lazarevic, V., X. Chen, J. H. Shim, E. S. Hwang, E. Jang, A. N. Bolm, M. Oukka, V. K. Kuchroo, and L. H. Glimcher. 2011. T-bet represses T(H)17 differentiation by preventing Runx1-mediated activation of the gene encoding RORgammat. *Nat. Immunol.* 12: 96–104.
15. Ono, M., H. Yaguchi, N. Ohkura, I. Kitabayashi, Y. Nagamura, T. Nomura, Y. Miyachi, T. Tsukada, and S. Sakaguchi. 2007. Foxp3 controls regulatory T-cell function by interacting with AML1/Runx1. *Nature* 446: 685–689.
16. Zheng, Y., S. Josefowicz, A. Chaudhry, X. P. Peng, K. Forbush, and A. Y. Rudensky. 2010. Role of conserved non-coding DNA elements in the Foxp3 gene in regulatory T-cell fate. *Nature* 463: 808–812.
17. Kitoh, A., M. Ono, Y. Naoe, N. Ohkura, T. Yamaguchi, H. Yaguchi, I. Kitabayashi, T. Tsukada, T. Nomura, Y. Miyachi, et al. 2009. Indispensable role of the Runx1-Cbfbeta transcription complex for in vivo-suppressive function of FoxP3+ regulatory T cells. *Immunity* 31: 609–620.
18. Rudra, D., T. Egawa, M. M. Chong, P. Treuting, D. R. Littman, and A. Y. Rudensky. 2009. Runx-CBFbeta complexes control expression of the transcription factor Foxp3 in regulatory T cells. *Nat. Immunol.* 10: 1170–1177.
19. Wong, W. F., M. Kurokawa, M. Satake, and K. Kohu. 2011. Down-regulation of Runx1 expression by TCR signal involves an autoregulatory mechanism and contributes to IL-2 production. *J. Biol. Chem.* 286: 11110–11118.
20. Egawa, T., R. E. Tillman, Y. Naoe, I. Taniuchi, and D. R. Littman. 2007. The role of the Runx transcription factors in thymocyte differentiation and in homeostasis of naive T cells. *J. Exp. Med.* 204: 1945–1957.
21. Naoe, Y., R. Setoguchi, K. Akiyama, S. Muroi, M. Kuroda, F. Hatam, D. R. Littman, and I. Taniuchi. 2007. Repression of interleukin-4 in T helper type 1 cells by Runx/Cbf beta binding to the Il4 silencer. *J. Exp. Med.* 204: 1749–1755.
22. Ichikawa, M., T. Asai, T. Saito, S. Seo, I. Yamazaki, T. Yamagata, K. Mitani, S. Chiba, S. Ogawa, M. Kurokawa, and H. Hirai. 2004. AML-1 is required for megakaryocytic maturation and lymphocytic differentiation, but not for maintenance of hematopoietic stem cells in adult hematopoiesis. *Nat. Med.* 10: 299–304.
23. Lee, P. P., D. R. Fitzpatrick, C. Beard, H. K. Jessup, S. Lehar, K. W. Makar, M. Perez-Melgosa, M. T. Sweetser, M. S. Schlissel, S. Nguyen, et al. 2001. A critical role for Dnmt1 and DNA methylation in T cell development, function, and survival. *Immunity* 15: 763–774.
24. Strasser, A., A. W. Harris, and S. Cory. 1991. bcl-2 transgene inhibits T cell death and perturbs thymic self-censorship. *Cell* 67: 889–899.
25. Damayanti, T., T. Kikuchi, J. Zaini, H. Daito, M. Kanehira, K. Kohu, N. Ishii, M. Satake, K. Sugamura, and T. Nukiwa. 2010. Serial OX40 engagement on CD4+ T cells and natural killer T cells causes allergic airway inflammation. *Am. J. Respir. Crit. Care Med.* 181: 688–698.
26. Soroosh, P., S. Ine, K. Sugamura, and N. Ishii. 2006. OX40-OX40 ligand interaction through T cell-T cell contact contributes to CD4 T cell longevity. *J. Immunol.* 176: 5975–5987.
27. Kanto, S., N. Chiba, Y. Tanaka, S. Fujita, M. Endo, N. Kamada, K. Yoshikawa, A. Fukuzaki, S. Orikasa, T. Watanabe, and M. Satake. 2000. The PEBP2beta/CBF beta-SMMHC chimeric protein is localized both in the cell membrane and nuclear subfractions of leukemic cells carrying chromosomal inversion 16. *Leukemia* 14: 1253–1259.
28. Kohu, K., H. Ohmori, W. F. Wong, D. Onda, T. Wakoh, S. Kon, M. Yamashita, T. Nakayama, M. Kubo, and M. Satake. 2009. The Runx3 transcription factor augments Th1 and down-modulates Th2 phenotypes by interacting with and attenuating GATA3. *J. Immunol.* 183: 7817–7824.
29. Trapnell, B. C., J. A. Whitsett, and K. Nakata. 2003. Pulmonary alveolar proteinosis. *N. Engl. J. Med.* 349: 2527–2539.
30. Puig-Kröger, A., C. Lopez-Rodriguez, M. Relloso, T. Sanchez-Elsner, A. Nueda, E. Munoz, C. Bernabeu, and A. L. Corbi. 2000. Polyomavirus enhancer-binding protein 2/core binding factor/acute myeloid leukemia factors contribute to the cell type-specific activity of the CD11a integrin gene promoter. *J. Biol. Chem.* 275: 28507–28512.
31. Holt, P. G., D. H. Strickland, M. E. Wikstrom, and F. L. Jahnsen. 2008. Regulation of immunological homeostasis in the respiratory tract. *Nat. Rev. Immunol.* 8: 142–152.
32. Campbell, J. J., C. E. Brightling, F. A. Symon, S. Qin, K. E. Murphy, M. Hodge, D. P. Andrew, L. Wu, E. C. Butcher, and A. J. Wardlaw. 2001. Expression of chemokine receptors by lung T cells from normal and asthmatic subjects. *J. Immunol.* 166: 2842–2848.
33. Kohlmeier, J. E., T. Cookenham, S. C. Miller, A. D. Roberts, J. P. Christensen, A. R. Thomsen, and D. L. Woodland. 2009. CXCR3 directs antigen-specific effector CD4+ T cell migration to the lung during parainfluenza virus infection. *J. Immunol.* 183: 4378–4384.
34. Kim, H. P., L. L. Korn, A. M. Gamero, and W. J. Leonard. 2005. Calcium-dependent activation of interleukin-21 gene expression in T cells. *J. Biol. Chem.* 280: 25291–25297.
35. Mehta, D. S., A. L. Wurster, A. S. Weinmann, and M. J. Grusby. 2005. NFATc2 and T-bet contribute to T-helper-cell-subset-specific regulation of IL-21 expression. *Proc. Natl. Acad. Sci. USA* 102: 2016–2021.
36. Spolski, R., and W. J. Leonard. 2008. Interleukin-21: basic biology and implications for cancer and autoimmunity. *Annu. Rev. Immunol.* 26: 57–79.
37. Korn, T., E. Bettelli, W. Gao, A. Awasthi, A. Jager, T. B. Strom, M. Oukka, and V. K. Kuchroo. 2007. IL-21 initiates an alternative pathway to induce proinflammatory T(H)17 cells. *Nature* 448: 484–487.
38. Nurieva, R., X. O. Yang, G. Martinez, Y. Zhang, A. D. Panopoulos, L. Ma, K. Schluns, Q. Tian, S. S. Watowich, A. M. Jetten, and C. Dong. 2007. Essential autocrine regulation by IL-21 in the generation of inflammatory T cells. *Nature* 448: 480–483.
39. Zhou, L., I. I. Ivanov, R. Spolski, R. Min, K. Shenderov, T. Egawa, D. E. Levy, W. J. Leonard, and D. R. Littman. 2007. IL-6 programs T(H)-17 cell differentiation by promoting sequential engagement of the IL-21 and IL-23 pathways. *Nat. Immunol.* 8: 967–974.
40. Linterman, M. A., L. Beaton, D. Yu, R. R. Ramiscal, M. Srivastava, J. J. Hogan, N. K. Verma, M. J. Smyth, R. J. Rigby, and C. G. Vinuesa. 2010. IL-21 acts directly on B cells to regulate Bcl-6 expression and germinal center responses. *J. Exp. Med.* 207: 353–363.
41. Ozaki, K., R. Spolski, R. Ettinger, H. P. Kim, G. Wang, C. F. Qi, P. Hwu, D. J. Shaffer, S. Akilesh, D. C. Roopenian, et al. 2004. Regulation of B cell differentiation and plasma cell generation by IL-21, a novel inducer of Blimp-1 and Bcl-6. *J. Immunol.* 173: 5361–5371.

42. Ozaki, K., R. Spolski, C. G. Feng, C. F. Qi, J. Cheng, A. Sher, H. C. Morse III, C. Liu, P. L. Schwartzberg, and W. J. Leonard. 2002. A critical role for IL-21 in regulating immunoglobulin production. *Science* 298: 1630–1634.
43. Zotos, D., J. M. Coquet, Y. Zhang, A. Light, K. D'Costa, A. Kallies, L. M. Corcoran, D. I. Godfrey, K. M. Toellner, M. J. Smyth, et al. 2010. IL-21 regulates germinal center B cell differentiation and proliferation through a B cell-intrinsic mechanism. *J. Exp. Med.* 207: 365–378.
44. Kitamura, T., N. Tanaka, J. Watanabe, and S. Uchida Kanegasaki, Y. Yamada, and K. Nakata. 1999. Idiopathic pulmonary alveolar proteinosis as an autoimmune disease with neutralizing antibody against granulocyte/macrophage colony-stimulating factor. *J. Exp. Med.* 190: 875–880.
45. Dranoff, G., A. D. Crawford, M. Sadelain, B. Ream, A. Rashid, R. T. Bronson, G. R. Dickersin, C. J. Bachurski, E. L. Mark, J. A. Whitsett, et al. 1994. Involvement of granulocyte-macrophage colony-stimulating factor in pulmonary homeostasis. *Science* 264: 713–716.
46. Stanley, E., G. J. Lieschke, D. Grail, D. Metcalf, G. Hodgson, J. A. Gall, D. W. Maher, J. Cebon, V. Sinickas, and A. R. Dunn. 1994. Granulocyte/macrophage colony-stimulating factor-deficient mice show no major perturbation of hematopoiesis but develop a characteristic pulmonary pathology. *Proc. Natl. Acad. Sci. USA* 91: 5592–5596.
47. Palmer, M. T., and C. T. Weaver. 2010. Autoimmunity: increasing suspects in the CD4+ T cell lineup. *Nat. Immunol.* 11: 36–40.
48. Herber, D., T. P. Brown, S. Liang, D. A. Young, M. Collins, and K. Dunussi-Joannopoulos. 2007. IL-21 has a pathogenic role in a lupus-prone mouse model and its blockade with IL-21R.Fc reduces disease progression. *J. Immunol.* 178: 3822–3830.
49. Joshi, A. D., D. J. Fong, S. R. Oak, G. Trujillo, K. R. Flaherty, F. J. Martinez, and C. M. Hogaboam. 2009. Interleukin-17-mediated immunopathogenesis in experimental hypersensitivity pneumonitis. *Am. J. Respir. Crit. Care Med.* 179: 705–716.
50. Vanaudenaerde, B. M., S. I. De Vleeschauwer, R. Vos, I. Meyts, D. M. Bullens, V. Reynders, W. A. Wuyts, D. E. Van Raemdonck, L. J. Dupont, and G. M. Verleden. 2008. The role of the IL23/IL17 axis in bronchiolitis obliterans syndrome after lung transplantation. *Am. J. Transplant.* 8: 1911–1920.